Homogenization of Geostationary Infrared Imager Channels for Cold Cloud Studies Using Megha-Tropiques/ScaRaB

Thomas Fiolleau, Rémy Roca, Sophie Cloché, Dominique Bouniol, Patrick Raberanto

AUTHOR QUERIES

AUTHOR PLEASE ANSWER ALL QUERIES

PLEASE NOTE: We cannot accept new source files as corrections for your article. If possible, please annotate the PDF proof we have sent you with your corrections and upload it via the Author Gateway. Alternatively, you may send us your corrections in list format. You may also upload revised graphics via the Author Gateway.

1) **Please be aware that authors are required to pay overlength page charges ($230 per page) if the article is longer than 6 pages. If you cannot pay any or all of these charges please let us know. GRS Society members receive a discounted rate of $200 per page.**

2) **This pdf contains 2 proofs. The first half is the version that will appear on Xplore. The second half is the version that will appear in print. If you have any figures to print in color, they will be in color in both proofs.**

3) **The "Open Access" option for your article expires when the article is published on Xplore in an issue with page numbers. Articles in "Early Access" may be changed to Open Access. If you have not completed your electronic copyright form (ECF) and payment option please return to Scholar One "Transfer Center." In the Transfer Center you will click on "Manuscripts with Decisions" link. You will see your article details and under the "Actions" column click "Transfer Copyright." From the ECF it will direct you to the payment portal to select your payment options and then return to ECF for copyright submission.**

AQ:1 = Please note that "viewing zenithal angle" has been changed to "viewing zenith angle" throughout the text for consistency.

AQ:2 = Please confirm or add details for any funding or financial support for the research of this article.

AQ:3 = Please confirm whether the edits made in the current affiliation of all the authors are correct.

AQ:4 = Please confirm the postal code for CNRS, Institut Pierre Simon Laplace, Université de Toulouse, and Laboratoire de Météorologie Dynamique.

AQ:5 = Please provide the expansions for SEVIRI and AMSU.

AQ:6 = Please check the sentence "The use of geophysical targets like …" for clarity.

AQ:7 = Please check and confirm whether the edits made are appropriate: "Some studies on these geometric effects discussed the different configurations of cloud fields."

AQ:8 = Please provide the organization name, organization location, and report no. for Refs. [11] and [12].

AQ:9 = Please provide the organization location and report no. for Ref. [19].

AQ:10 = Please provide the volume no. for Ref. [25].

AQ:11 = Please provide the organization name and organization location for Refs. [30] and [31].

AQ:12 = Please provide the year of completion when the author Rémy Roca received the M.S. degree.

AQ:13 = Please provide the year of completion when the author Sophie Cloché received the M.S. degree.

AQ:14 = Please provide the location for CETP.

Homogenization of Geostationary Infrared Imager Channels for Cold Cloud Studies Using Megha-Tropiques/ScaRaB

Thomas Fiolleau, Rémy Roca, Sophie Cloché, Dominique Bouniol, and Patrick Raberanto

***Abstract*— Infrared (IR) observations from the fleet of multiagencies meteorological geostationary satellites have a great potential to support scientific and operational investigations at a quasi-global scale. In particular, such a data record, defined as the GEOring data set, is well suited to document the tropical convective systems life cycles by applying cloud tracking algorithms. Yet, this GEOring data set is far from being homogeneous, preventing the realization of its potential. A number of sources of inhomogeneities are identified ranging from spatiotemporal resolutions to spectral characteristics of the IR channels and calibration methodologies. While previous efforts have attempted to correct such issues, the adjustment of the cold part of the IR spectrum remains unfit for cold cloud studies. Here, a processing method is introduced to minimize the inhomogeneities against a reference observational data set from the Scanner for Radiation Budget (ScaRaB) instrument onboard the Megha-Tropiques satellite. The method relies on the collocations between the geostationary observations and the reference. The techniques exhibit significant sensitivity to the selection of the relevant pairs of observations requiring a dedicated filtering of the data. A second effort is then proposed to account for the limb-darkening effect and a method is developed to correct the brightness temperature (BT) dependence AQ:1 on the geostationary viewing zenith angle (VZA). Overall, results show a residual after the processing of 0 K between any of the geostationary data and the ScaRaB reference. The final calibrated and limb-adjusted IR observations are then homogeneous for cold BT lower than 240 K with a standard deviation lower than 1.5 K throughout the GEOring.**

***Index Terms*— Calibration and spectral corrections, cold cloud studies, geostationary satellites, infrared (IR) image sensors, limb-darkening corrections.**

I. Introduction

METEOROLOGY agencies monitor individually operational geostationary platforms, which when used all together permit an observation for all longitudes of the Earth on a large latitudinal band (∼60° S–60° N) with similar instruments. The potential benefit of such an observing capability has triggered numerous efforts in the past 40 years to make use of it for various applications, ranging from the elaboration of a unique perspective on clouds studies [1], [2] for precipitation estimation [3], climate studies [4], and global visualization applications [5]. Yet, when carefully examined, this GEOring appears to be far from a homogenous suite of instruments operated in a similar fashion. The space/time resolution and sampling differ across the platforms. The acquisition procedure also differs among the satellites (from South to North, North to South, or by sector). The calibration procedure of each instrument is also performed at the individual level with the instruments' specific modes of operation. Since 2011, for the infrared (IR) channels, the agencies provide alternative calibration coefficients obtained from a statistical comparison to hyperspectral IR measurements from low earth-orbiting satellites using the common methodology of the Global Space-Based InterCalibration System (GSICS) [6]. Nevertheless, the GSICS currently only provides calibration coefficients referenced to the NASA Earth Observing System (EOS), Aqua Atmospheric IR Sounder (AIRS), and the Exploitation of Meteorological Satellites (EUMETSAT)–Centre National d'Etudes Spatiales (CNES), Meteorological Operation (MetOp), and IR Atmospheric Sounding Interferometer (IASI) calibration standard. This harmonization effort does not take into account spectral band responses and viewing angle effects, which are needed for sensor homogenization. Indeed, while often referred to as a unique IR channel, the multiple instruments do show some spectral differences as well.

Most of the spectral imagers onboard geostationary satellites monitor with a relatively high temporal frequency the calibration coefficients for thermal IR channels by using onboard blackbody references. Some of the differences in the temperature measurements from one geostationary satellite to another can be explained by the differences in the calibration references, methods, as well as in the spectral filter functions. Moreover, it has been observed that the spectral imagers may degrade over time with different rates [7], [8]. The geostationary imagers can also be affected by short-term variations. The accumulation of ice on the surface of the imager optics modifies their spectral response function (SRF) and consequently affects the measurement of the temperatures. To face these issues, decontamination events are regularly applied to the radiometers inducing

AQ:2 Manuscript received July 17, 2019; revised November 25, 2019 and January 22, 2020; accepted February 4, 2020. *(Corresponding author: Thomas Fiolleau.)*

AQ:3 Thomas Fiolleau and Rémy Roca are with the Laboratoire d'Etudes en Géophysique et Océanographie Spatiales, CNRS, 31400 Toulouse, France (e-mail: thomas.fiolleau@legos.obs-mip.fr; remy.roca@legos.obs-mip.fr).

Sophie Cloché is with CNRS, Institut Pierre Simon Laplace, 75252 Paris, France (e-mail: sophie.bouffies-cloche@ipsl.fr).

AQ:4 Dominique Bouniol is with the Centre National de Recherches Météorologiques, CNRS, Météo-France, Université de Toulouse, 31057 Toulouse, France (e-mail: dominique.bouniol@meteo.fr).

Patrick Raberanto is with the Laboratoire de Météorologie Dynamique, CNRS, 75016 Paris, France (e-mail: patrick.raberanto@lmd.polytechnique.fr).

Color versions of one or more of the figures in this article are available online at http://ieeexplore.ieee.org.

Digital Object Identifier 10.1109/TGRS.2020.2978171

TABLE I
SUMMARY OF THE TECHNICAL CHARACTERISTICS OF THE VARIOUS EXISTING IR GEORING DATA SETS

Products	Spatial resolution	Temporal resolution	Spatial coverage	Temporal coverage	Calibration and temporal normalization	Limb darkening correction	Data source
Gridsat-B1	0.07°	180 min	70°S-70°N	1980-present	HIRS channel 8 [14]	Yes	ISCCP-B1
CPC	~ 0.04°	30 min	60°S-60°N	2000–present	No absolute calibration and no temporal normalization	Yes	Native
CLAUS	0.5°	180 min	Global*	1983-2006	ISCCP- B3	Yes	ISCCP-B3
CLAUS	0.3°	180 min	Global*	1985–2008	ISCCP- B3	Yes	ISCCP-B3
ISCCP-B1	Native FoV subsampled to ~ 0.1°	180 min	70°S-70°N	1980-present	AVHRR channel 5 [13]	No	Native
ISCCP-B3	Native FoV subsampled to ~ 0.3°	180 min	70°S-70°N	1983-2009	AVHRR channel 5 [13]	No	Native
This study	0.04°	30 min	35°S-35°N	2012-2016	SCARAB-IR channel 4	yes	Native

instability in the temperature measurements [9]. This effect has been particularly shown for the Meteosat Visible IR Imager (MVIRI) onboard the Meteosat-7 geostationary platform.

A diurnal cycle effect can also affect the imager calibration, especially for the instruments on the three-axis stabilized geostationary platforms [7], [9]. It has been shown that the sun-synchronous orbits of MetOp/IASI and EOS/AIRS used in the GSICS calibration are not sufficient to completely correct the diurnal IR calibration issues [10]. The precessing orbit of the tropical rainfall measuring mission (TRMM) platform and the observations of its visible and IR scanner (VIRS) have then been used to quantify and correct such a midnight IR calibration anomaly [10]. IR observations are also dependent on the geostationary viewing zenith angle (VZA). The issue is called limb darkening, corresponding to a decrease in the temperature as the VZA increases.

These multiple sources of inhomogeneity have prevented the full use of this unique observational capability, although a number of successful projects have attempted to overcome the above-listed limitations. Indeed, a number of significant efforts have been proposed in the last two decades to produce more or less homogeneous "global" archive of geostationary data sets for various applications. It ranges from cloud climatology computations (International Satellite Cloud Climatology Project (ISCCP)-B1, ISCCP-B3, and Cloud Archive User Service (CLAUS) [11]), hurricane trend analysis, support of precipitation estimation (Gridded Satellite (GridSat) [12]), real-time monitoring of precipitation (Climate Prediction Center (CPC) [13]), for the enhancement of radiation budget averages [8]. Additional information on these GEOring data sets is listed in [4]. Table I summarizes the available IR GEOring data sets altogether with their respective properties and homogeneity levels. The ISCCP-B1 and B3 have been subsampled to a 180-min temporal resolution and to, respectively, ~0.1° and ~0.3° spatial resolution. They have been calibrated and spectrally normalized using advanced very high-resolution radiometer (AVHRR) observations [14]. The CLAUS data sets rely on the ISCCP-B3 and have been reprojected to an equal angle map projection with a spatial resolution of 0.3° and 0.5°. The GridSat-B1 is based on the ISCCP-B1 data set remapped to a 0.07° regular grid. In addition to the intercalibration used for the ISCCP data set, a second calibration using the high-resolution IR radiation sounder (HIRS) observations has been applied to correct a bias at cold temperatures observed after 2001. The CPC product is built in real time from native geostationary observations. The data are remapped to a regular grid of ~0.04° spatial resolution and are available every 30 min. To reduce the spectral differences and calibration issues, a complex, multistep, multiregional procedure is applied by comparing the brightness temperatures (BTs) from pairs of geostationary platforms. However, this procedure does not provide any absolute calibration. Also note that a limb correction has been performed on the GridSat-B1, CPC, and CLAUS data. In short, while a number of efforts have paved the way for a quantitative use of the GEOring data sets, no dedicated effort toward the cold BT regimes has been promoted so far. Yet, cold cloud studies benefit a lot from geostationary IR observations, for cloud microphysical or macrophysical parameters retrievals. The spatiotemporal resolution of the measurements further allows the life cycle analysis of the cold cloudiness and the estimation of related parameters. The present GEOring attempt is directed toward these scientific applications. In particular, it will serve as the input of the realization of a tropical mesoscale convective system data set using the TOOCAN algorithm [15].

TABLE II

TECHNICAL CHARACTERISTICS OF THE OPERATIONAL GEOSTATIONARY SATELLITES FLEET AND THE ASSOCIATED IMAGERS USED OVER THE 2012–2016 PERIOD

Platform	Nadir location	Instrument	Central wavelength	Spectral interval	Spatial resolution at nadir	Temporal resolution	Region of interest	Source	Period
GOES-15	135° W	IMAGER	10.7 µm	10.2-11.2 µm	4 km	30 min	180° W-105° W 35° S-35° N	NOAA / DWD	Jan 2012-Dec 2016
GOES-13	75° W	IMAGER	10.7 µm	10.2-11.2 µm	4 km	30 min	111° W-30° W 35° S-35° N	NOAA / DWD	Jan 2012-Dec 2016
METEOSAT-8/9/10	0°	SEVIRI	10.8 µm	9.8-11.8 µm	3 km	15 min	45° W-45° E 35° S-35° N	EUMETSAT/ AERIS	Jan 2012-Dec 2016
METEOSAT-7 (IODC)	57.5° E	MVIRI	11.5µm	10.5-12.5 µm	5 km	30 min	12° E-107° E 35° S-35° N	EUMETSAT/ AERIS	Jan 2012-Dec 2016
MTSAT-2	145° E	IMAGER	10.8 µm	10.3-11.3 µm	4 km	30 min	94° E-170° W 35° S-35° N	AERIS/ CIMSS	Jan 2012-May 2015
HIMAWARI-8	140.7° E	AHI	11.2 µm	11.0-11.4 µm	2 km	10 min	94° E-170° W 35° S-35° N	AERIS/ JMA	Jun 2015-Dec 2016

Such analyses require observations with a minimal temporal resolution of 30 min [15], [16] to ensure tracked objects overlap between two images. Such kind of studies requires the use of thresholds applied to BT, ranging from 200 to 240 K, depending upon the analysis [17], [15]. A homogeneous data set is then mandatory, if one wants to proceed with the whole tropical belt. The homogeneity and basic requirements for a GEOring IR data set geared toward tropical cold cloud tracking applications can be summarized as follows:

1) High-resolution spatial footprint and high spatial resolution (∼5 km).
2) A minimum of 30 min time sampling.
3) A spatial coverage dedicated to the tropics.
4) Homogenized BTs through spectral and calibration adjustment.
5) Limb adjustment of IR observations.

Matching these requirements with the specifications of the IR data sets summarized in Table I confirms the need for a dedicated level 1c GEOring IR tailored for cold cloud tracking applications. Moreover, the current implementation of the GSICS coefficients computation is directed toward the warm part of the spectrum [8], ruling out its use for cold cloud studies calling for an alternative, cold cloud compliant, absolute calibration reference for the GEOring. The limb effect is less strong over the cold part of the temperature spectrum than at the warm and clear sky end of the spectrum, and the limb correction is easier to set up for cold cloudy scenes (BTs < 240 K) than for the clear atmosphere. This effect is strongly nonlinear and is thought to be impactful only for the viewing angle above 26.5° [11]; it may still require a correction for a homogeneous interpretation of the BT field all through the image. It is difficult to establish requirements once and for all in terms of residuals difference in the homogeneous data, based on the radiometric noise of the first generation sensors and the various sources of uncertainties in the adjustment procedure and basic cloud-oriented retrievals sensitivity. We propose to target a less than 1.5 K standard deviation among any of the two geostationary satellites in the final calibrated and limb-adjusted product for BTs < 240 K.

II. DATA

A. Five-Year Database of IR Geostationary Observations Over the Entire Tropics

Thermal channel BT images obtained by the operational meteorological geostationary satellite fleet are used over the 35°S–35°N latitude belt and for the whole 2012–2016 period. Table II shows the geostationary IR data used to cover the entire tropics for this period. The geostationary data set has been collected from different sources: the U.S. National Oceanic and Atmospheric Administration (NOAA), the European Organization for the Exploitation of Meteorological Satellites (EUMETSAT), the Japan Meteorological Agency (JMA), and the French Atmosphere and Service Data Pole (AERIS). Note that the Multifunctional Transport Satellite (MTSAT) data set has also been completed from the Space Science and Engineering Center (SSEC) of the University of

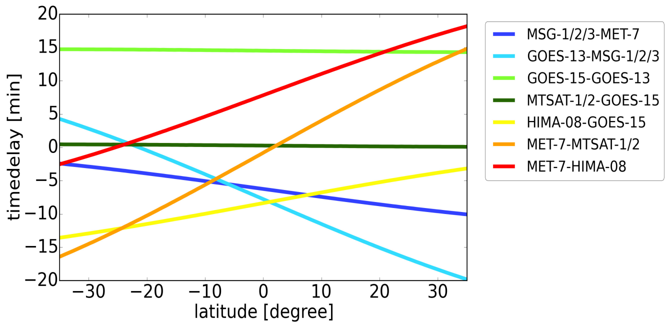

Fig. 1. Time delay of acquisition between pairs of geostationary images according to the latitude.

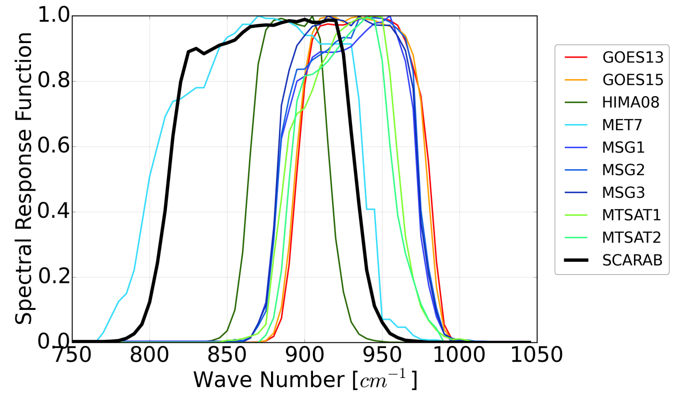

Fig. 2. SRF of the IR channel of the GEOring. The black line is the spectral response of the channel 4 of the ScaRaB instrument.

Wisconsin–Madison. The technical characteristics of each geostationary platform and their imagers are described in Table II and can differ from one platform to another. First, considering the temporal resolution, Meteosat Second Generation (MSG) and HIMAWARI-8 observe the Earth, respectively, with a 15- and 10-min time resolution, while the other platforms display a 30-min temporal resolution. Similarly, the scan-times vary from 7 min for HIMAWARI-8 to 25 min for Meteosat-7. The Geostationary Operational Environmental Satellite (GOES)-13 and GOES-15 sensors follow a complex scanning sector schedule. The full disk images are produced every 3 h, while the northern hemisphere and the southern hemisphere images are produced every 30 min with a time lag of few minutes between each scan. Also, note that the scanning schedule of MTSAT-2 does not provide half-hourly sampling of the southern hemisphere region. Contrary to the other imagers, the GOES-13 imager starts its earth scan at 15 and 45 min of the hour. Also note that Meteosat first- and second-generation imagers start their earth scan from the southeast corner, whereas NOAA and JMA platforms begin their earth scan from the northwest corner. All these temporal scanning differences imply some time delays between neighboring platforms observing the same region (Fig. 1). While the 15-min time delay is constant for the pairs of the GOES-15/GOES-13 and MTSAT-2/GOES-15 platforms, the time delay varies according to the latitude for the other pairs of geostationary platforms. At 35° S, a maximum time delay is found for the pair of MSG/GOES-13 platform of around 20 min. The maximum time delay amplitude accounted for the pair of the Meteosat-7/MTSAT-2 platforms and varies between −16 and 15 min.

Depending on the considered satellite, spatial resolution at nadir differs from one geostationary satellite to another and ranges from 2 km for HIMAWARI-8 to 5 km for Meteosat-7. In addition to the resolutions disparities, the GEOring is also characterized by differences in the central wavelength and the associated SRFs of each of the instruments (Fig. 2). While the central wavelength ranges between 10.7 and 11.5 μm for the GOES imagers and the Meteosat-7 imager, respectively, two types of SRFs can define the IR channels. The GOES-13, GOES-15, MTSAT-2, and HIMAWARI-8 imagers display narrowband channels with a bandwidth lower than 1 μm, whereas AQ:5 the Meteosat-7/MVIRI and MSG/SEVIRI imagers exhibit broader channels characterized by a 2 μm bandwidth. A broadband channel is highly sensitive to ice contamination on the optics of the imagers, modifying their SRFs, and consequently, introducing a calibration error. Operational decontamination procedures are applied regularly to remove the ice build-up on the optics. Thus, spectral differences, as well as the individual satellite calibration procedures, contribute to the GEOring radiometric inhomogeneities.

B. *Megha-Tropiques/ScaRaB-3 Observations*

The Scanner for Radiation Budget (ScaRaB) instrument on the Megha-Tropiques platform [18] is the third of its kind [19], [20] and has been designed to measure the Earth radiation components at the top of the atmosphere with high accuracy (<1%). The instrument acquires data across the satellite track with a swath of ∼2200 km from 30° S to 30° N. It is a broadband radiometer with four channels. The total channel measures the total energy between 0.2 and 100 μm. The shortwave channel (0.2–4 μm) is subtracted from the total channel to obtain the longwave part of the spectrum [21]. The fourth channel is an IR thermal channel (10.5–12.5 μm) which is used in this article (Fig. 2). The instrument operates nominally since the beginning of the mission and its operational performances are well in line with the specifications [22]–[24]. The nominal resolution of the ScaRaB footprint at nadir is 40 km and is detailed in [18].

The stability of the instrument is monitored by the CNES on a daily basis and so far, the Megha-Tropiques instruments have shown remarkable stability [25]. AQ:6 The use of geophysical targets like deep convective clouds (DCC) has been shown to be useful for geophysical calibration and cross-calibration of either broad radiometers [26], [27]. It is used here to showcase the relative stability of the channel 4 to that of the longwave channel. Fig. 3 shows the ratio between the radiance in channel 4 and channel 1 over the studied period for various deep convective regimes. The two channels of the instrument show no sign of relative degradation and a very steady behavior. Comparisons with the Clouds and the Earth's Radiant Energy System (CERES) instrument using dedicated collocation campaigns [28] further indicate a very good agreement between the two instruments' longwave channels [29].

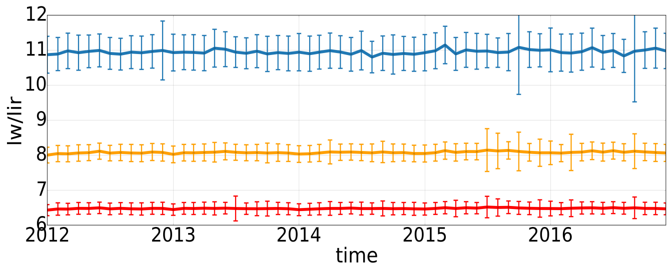

Fig. 3. Evolution of the ratio between measured radiance in the longwave band and in the IR channel of ScaRaB over the 2012–2016 period for various deep convective regimes. The blue curve corresponds to an IR radiance lower than 2.25 $\mathrm{W \cdot m^{-2} \cdot sr^{-1}}$ corresponding to a 187 K BT, the yellow one lower than 4.25 $\mathrm{W \cdot m^{-2} \cdot sr^{-1}}$ (207.4 K), and the red curve corresponds to an IR radiance lower than 7.75 $\mathrm{W \cdot m^{-2} \cdot sr^{-1}}$ (224.5 K).

The ScaRab instrument is also thermally controlled and is not impacted by icing events as shown in the monitoring of the instrument performances [22], [23]. The combination of an accurate and stable instrument makes it a well-suited reference to adjust the geostationary data.

Here we use the so-called level 2B products that consist of a 0.5° regularly gridded instantaneous directional radiances ($\mathrm{W \cdot m^{-2} \cdot sr^{-1}}$). The original measurements are averaged on the regular grid using a statistical technique and the point spread function of the instrument [30]. Since 2011, the availability of this product is about 99.9%, making it a useful resource as a reference instrument for the spectral homogenization of the GEOring data. Note that unlike sun-synchronous platforms, the precessing orbit of Megha-Tropiques samples all the local times every 51 days allowing the collocation with the geostationary data all through the day and then the correction of the midnight IR anomaly [10], [18], [31]. The low inclination at the equator (20°) and high altitude of flight (865 km) also allow high repetitive measurements in the tropics [18].

III. Homogenous Level 1c IR Data Set for the Tropics for 2012–2016

A. Homogenization of the Temporal Resolution

Given the requirements for cold cloud studies (see Section I), the lack of temporal resolution homogeneity between the geostationary imagers is accounted for by using a 30-min temporal frequency for all the platforms, preventing the use of MTSAT data in the southern hemisphere.

B. Homogenization of the Spatial Resolution

A common equal angle grid of 0.04° × 0.04° has been selected for all the platforms to account for this source of inhomogeneity. This resolution is very close to the native resolution of GOES-13, GOES-15, MTSAT-2, and Meteosat-7 data. The regridding process is performed by applying the inverse distance weighting method in the radiance space with a maximum search radius corresponding to the sum of half of the geostationary spatial resolution for a given pixel plus a half of the equal angle grid resolution. Then, the average radiance is transformed in BT using the Planck function in order to account for its nonlinearity.

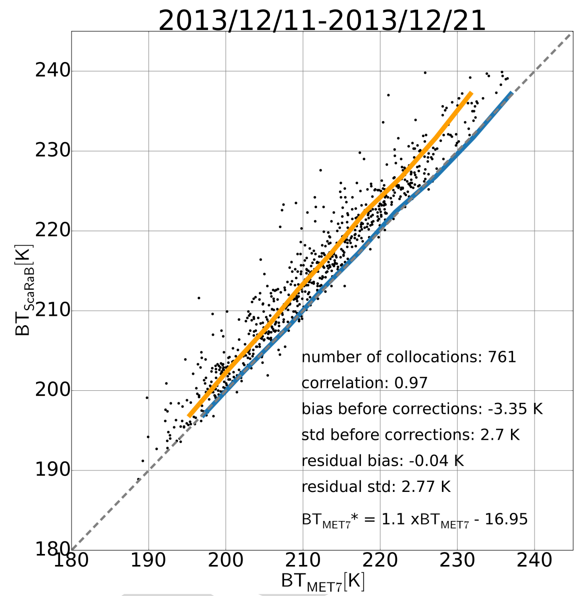

Fig. 4. Scatter plot between BT_{MET7} and BT_{ScaRaB} obtained after the filtering procedure over a ten-day period starting in 2013/12/11 for BT in the range [180–240 K]. The orange line corresponds to the average BT for each 5 K bin. The blue line corresponds to the residual bias.

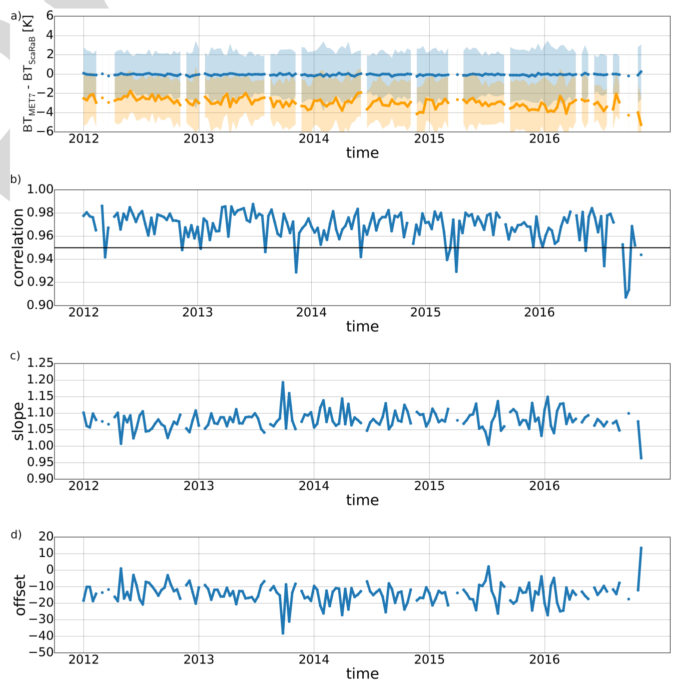

Fig. 5. (a) Time series of decadal initial BT bias (orange) and corrected BT bias (blue) for Meteosat-7 IR observations with respect to ScaRaB in the range [180–240 K]. The filled and transparent areas in orange and blue represent the standard deviations: (b) Time series of decadal linear regression correlations, (c) slope, and (d) offset between the ScaRaB and the Meteosat-7 IR observations in the range [180–240 K].

C. Intercalibration and Spectral Normalization

1) Regression Technique: The use of a common low earth-orbiting satellite, carrying an IR radiometer to anchor each of the platforms to a common reference data set, forms the basis of the different intercalibration and normalization

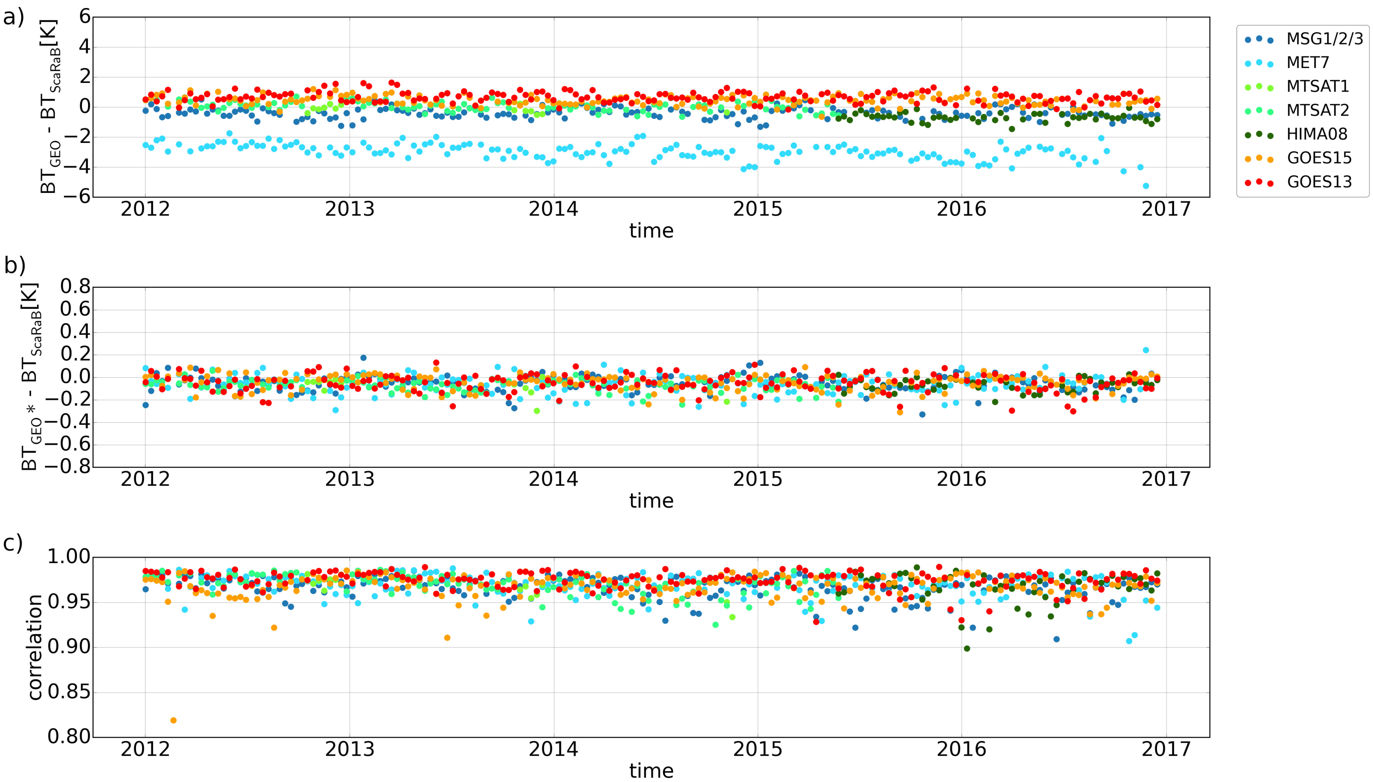

Fig. 6. (a) Time series of initial BT bias of geostationary IR observations with respect to ScaRaB in the range [180–240 K]. (b) Time series of BT bias between the geostationary IR observations and the ScaRaB observations in the range [180–240 K] after spectral and calibration corrections. (c) Time series of correlations between the ScaRaB and the geostationary IR observations in the range [180–240 K]. Each dot corresponds to a ten-day period.

efforts listed in Table I [14], [32] or under the GSICS calibration procedure [7]. Regression-based techniques are the most commonly used approaches. The difficulty arises in building the pairs (space/time/angular collocation) as well as in selecting the pairs of observations that will be regressed. This selection can have a strong impact on the result. Hence, it has been noted that the original ISCCP intercalibration was skewed toward a warm scene due to the implementation of the pairs selection filter prior to the regression computation, yielding a ~4 K cold bias on the cold part of the spectrum [33]. Similarly, most of the tropical observations are located over large BT values and only a few of them are explained by DCCs. As the larger population of collocations is explained by high BT, the GSICS corrections are optimized for clear sky conditions and are not well suited for the cold cloud scenes [7]. A specific homogenization of the IR geostationary database is then required to fit with the objective of cold cloud tracking applications. This homogenization consists of a spectral normalization as well as an intercalibration of the various geostationary imagers focused on high cold clouds and on cold BTs. For this purpose, the BTs from the geostationary imagers are calibrated and spectrally normalized against the ScaRaB channel 4 measurements. The final data set then consists of a 10.5–12.5 μm IR equivalent BT. Calibration uncertainty is expected to be within 1 K, which is the typical error for operational satellite calibration [34]. Contrary to other geostationary imagers, the correction of the Meteosat-7/MVIRI imager is restricted to an intercalibration procedure, since its broad SRF is similar to the ScaRaB/channel 4 and both of them are centered on 11.5 μm.

2) Selection of the Data Match-Ups for the Regression: The IR geostationary data from all the platforms are first remapped from their native formats to a regular lon/lat 0.5° grid every 30 min to allow direct comparison with the ScaRaB/L2B data. Prior to computing the averaged radiance and the associated spatial standard deviation for each 0.5° grid point, the BTs of each geostationary platform are converted in radiances (mW $\cdot$ $m^{-2}\cdot sr^{-1}\cdot cm^{-1}$) by applying the Planck function. The information on geostationary scan-time is also indicated for every grid point. The collocation between the ScaRaB-L2B observation and the IR 0.5° × 0.5° gridded geostationary data is reached when both view the same scene with a predefined time delay and similar viewing geometry. The predefined criteria are.

1) A maximum VZA of 20° and 26°, respectively, for the ScaRaB and the geostationary observation, to ensure alignment of the collocated pixels in viewing geometry and to avoid limb-darkening issues [35].
2) A maximum time delay of 10 min between two collocated pixels, which is a tradeoff between a relevant number of match-ups to populate the decadal regressions and the best possible temporal precision.
3) The IR-gridded radiances are regressed in units of temperature.

As we focus on high cold clouds scenes, we have developed a filtering procedure that keeps more collocation scenes at a colder temperature. Indeed, a bulk of collocations occurs at

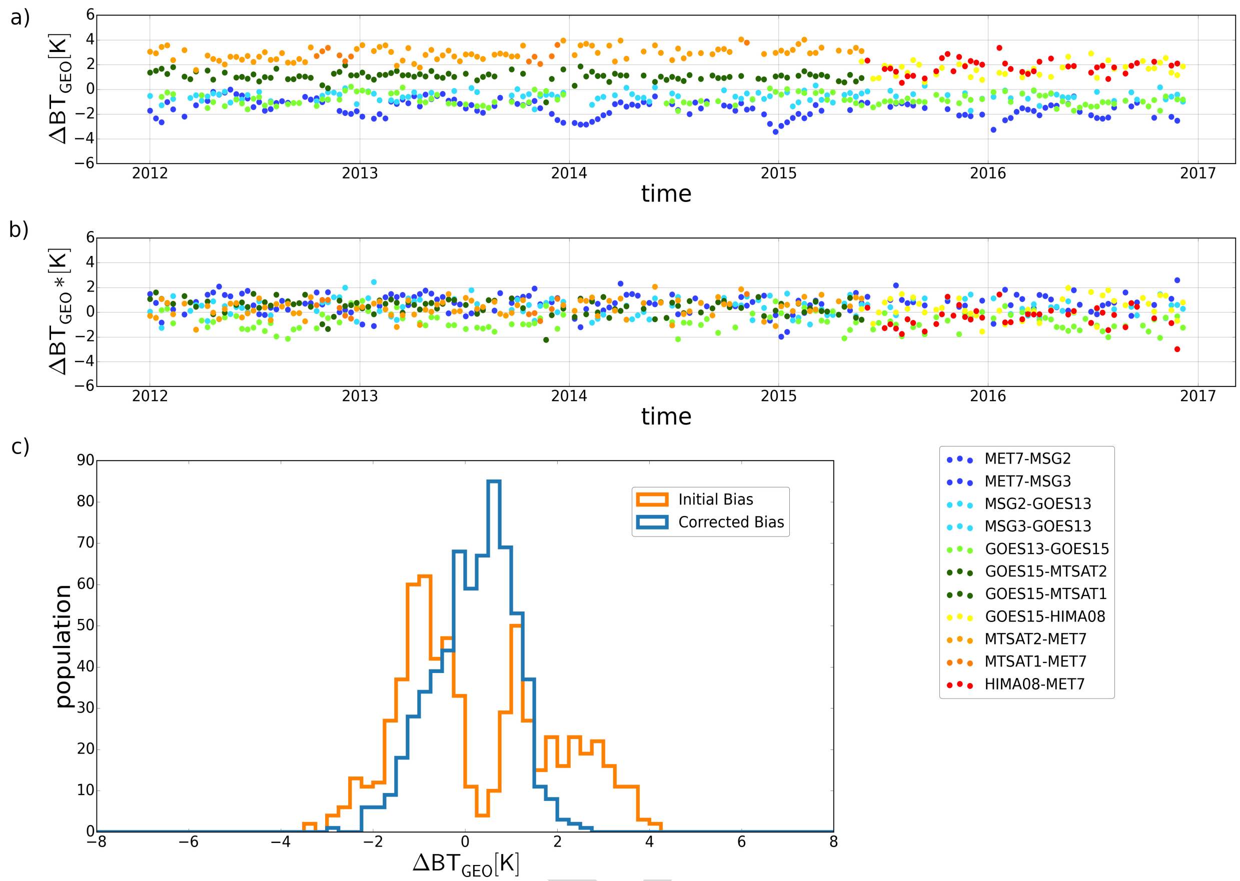

Fig. 7. (a) Time series of initial BT bias between pairs of geostationary platforms observing common areas with an equivalent VZA in the range [180–240 K]. (b) After spectral and calibration corrections; each dot corresponds to a ten-day period. (c) Distribution of the bias before and after corrections over the 2012–2016 period for all the pairs of geostationary platforms for all the ten-day periods.

a warmer temperature and displays a lower standard deviation [33]. To separate the high cold cloud population from the warmer targets in the scatterplot, thresholds are applied to the GEO standard deviation that depends on the BT. Pixels presenting a $BT_{GEO} > 240$ K are rejected if their standard deviations are larger than 0.5 K and pixels with $BT_{GEO} < 240$ K are kept if their standard deviations are lower than 2 K. Besides separating the high cold cloud population from clear sky pixels, this filtering procedure ensures that heterogeneous moving objects do not contaminate the collocation scenes and that the two instruments observe the same high cloud target. Assuming also that the IR radiometers onboard geostationary platforms have a linear response when observing high cold cloud homogeneous scenes [8], [36], the calibration and spectral normalization corrections are then based on linear regressions computed over a 180 –240 K range. For this, the collocated BT_{GEO} and BT_{ScaRaB} are binned and averaged for every BT_{ScaRaB} interval of 5 K from 180 to 240 K. The regression coefficients are then computed over these binned data every ten days and over a ten-day period. This is required to ensure statistical robustness but prevent higher frequency variation (<10 days) of the calibration issues (due to decontamination for instance) to be accounted for. As shown below, such higher frequency effects do not impact the residuals of the regression. Correlations are used to determine the ten-day period that might have match-ups errors. If the correlations are lower than 0.95 or if the population of collocations does not exceed ten matchups, we consider that the linear regression cannot be computed and that every ten-day period is removed from our analysis. In this case, the previous regression coefficients are replicated.

3) Results: Fig. 4 shows an example of such a regression computed from 761 collocated pixels between the Meteosat-7/MVIRI imager and the Megha-Tropiques/ScaRaB observations acquired over a ten-day period from 2013/2012/2011 and for a range between 180 and 240 K. The 11.5 μm channel of Meteosat-7 exhibits a large negative bias (-3.35 K) for this considered BT and for this specific period. The blue line shows the regression fit given by a slope of 1.11 and an offset of -16.95 K. The correction has produced a very low residual bias, which averages at -0.04 K over this decadal period, and the correlation higher than 0.97 between the two data sets shows the high quality of the regression computation. Fig. 5(a) shows the time series of difference between Meteosat-7/MVIRI and ScaRaB before and after calibration over the 2012–2016 period. The Meteosat-7 BT is corrected every ten days using the slopes and offset computed from the linear regression. Over the period and for the specific Meteosat-7 geostationary platform, 12% of the decadal scatterplots are excluded from our analysis following

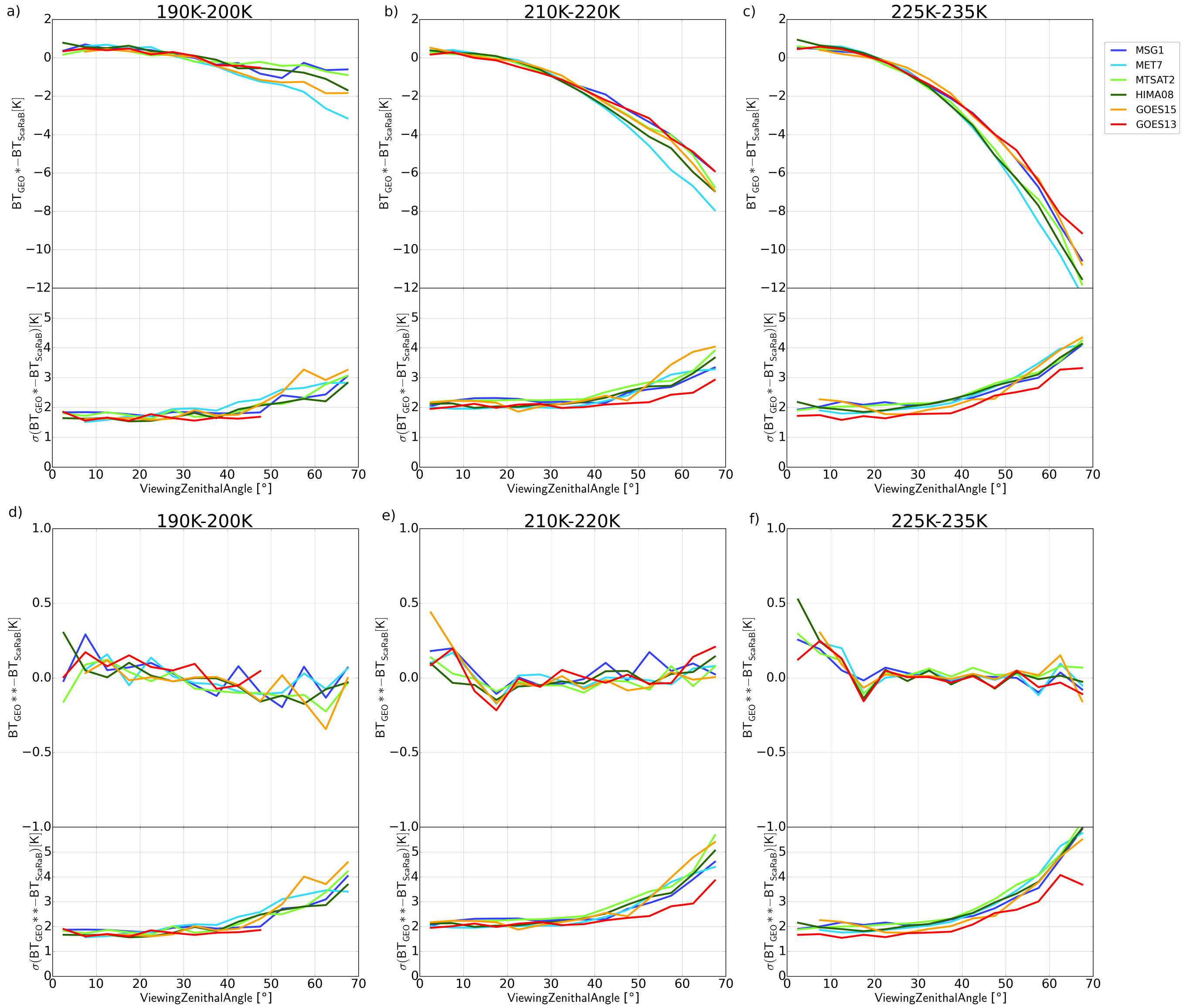

Fig. 8. Variation of the BT bias and the corresponding standard deviation between the GEO and the SCARAB observations according to the geostationary VZA, for a $VZA_{ScaRaB} < 20°$ and for three different ranges of BT_{ScaRaB}. (a)–(c) Before VZA corrections. (d)–(f) After VZA corrections.

the filtering procedure [Fig. 5(b)] and 87 405 collocations have then been used to compute the decadal regressions. One can observe that over the 2012–2016 period, and before the corrections, the Meteosat-7/MVIRI exhibits a negative bias, averaging at −2.98 K and negatively increasing slightly with time due to contamination on the optics. This radiometric issue has been fully documented in [7]. The variations of the slopes and offsets are relatively stable over the period [Fig. 5(c) and (d)], showing the robustness of the methodology. After applying the calibration correction, the residual bias is very smooth, stable, and close to zero over the whole period. The calibration and spectral normalization corrections are applied on all the geostationary platforms available over the 2012–2016 period. The results have been obtained over the entire period, and for all the geostationary platforms by filtering 8% of the decadal scatterplots which did not pass our quality control [Fig. 6(c)], leading to a comparison of around 655 000 collocations. Fig. 6(a) shows the time series of the decadal initial bias in BT for all the geostationary imagers with respect to the ScaRaB observations in the range 180–240 K. Over the 2012–2016 period, the Meteosat-7/MVIRI exhibits the highest error as discussed previously. It is also to be noted that the MSG/SEVIRI imager shows a relatively high negative bias (−1.39 K) to be compared to the other instruments whose biases are mainly in the range −0.5–0.5 K over the entire period. While the calibration issues only explain the bias between Meteosat-7 and ScaRaB, the differences of temperature between ScaRaB and the other geostationary platforms can be explained by both a poor calibration and some differences in the SRF. The results of the intercalibration and spectral normalization are shown in Fig. 6(b). Over the entire period and for all the geostationary platforms, the decadal

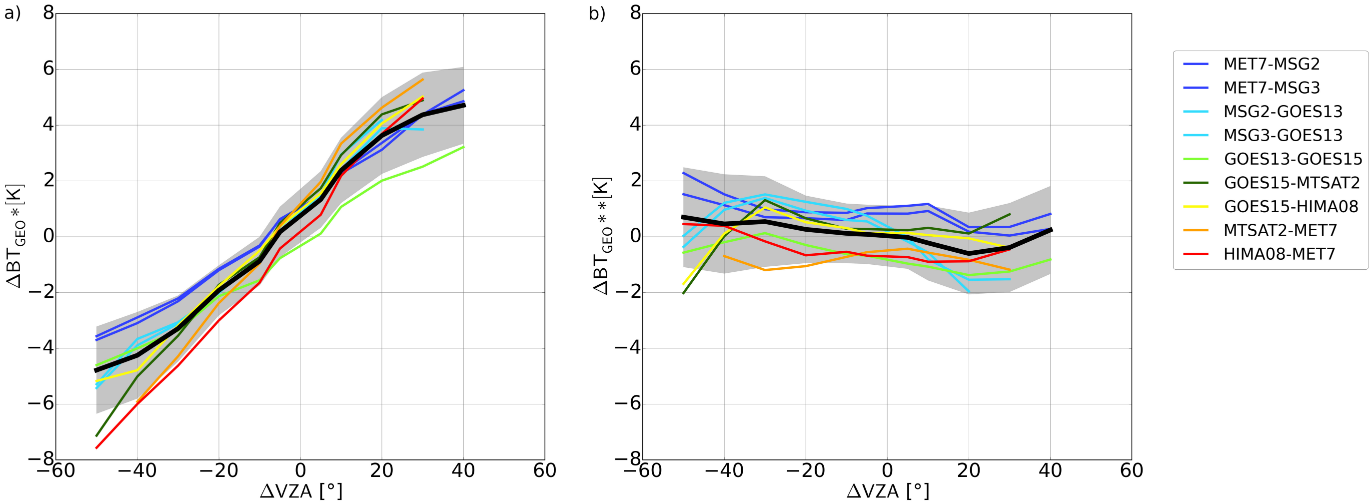

Fig. 9. Variation of the BT bias according to the VZA differences between pairs of geostationary platforms observing common areas and for BT_{ScaRaB} in the range [180–235 K]. (a) Before VZA corrections. (b) After VZA corrections. The BT bias and its standard deviation for all the pairs of geostationary platforms are represented respectively by the black line and the filled area in gray over the 2012–2016 period for all the ten days.

residual bias indicates a very low and stable bias, around 0 K, with a standard deviation lower than 0.08 K between BT_{ScaRaB} and BT_{GEOS}. The corrections are then directly applied to the original geostationary data.

To fully describe the impact of the ScaRaB calibration and spectral corrections, an independent validation has been developed. The bias of uncorrected and corrected BT_{GEO} is then computed in the range of 180–240 K every ten days between pairs of neighbored geostationary platforms observing common areas and sharing an equivalent VZA (Fig. 7). Indeed, for two adjacent geostationary satellites, the BT bias at the middle of the overlap region should average to zero, due to the similar geometry for both platforms. Fig. 7(a) shows the time series of decadal mean differences between uncorrected BTs of each pair of geostationary satellites. Each color represents a pair of geostationary platforms. Results indicate a scatter of the decadal bias between −4 and 4 K. The maximum bias occurs for the BT differences between MTSAT-1/2 and Meteosat-7, which averages at 2.9 K from the beginning of 2012 to June 2015. The bias between uncorrected BT_{MET-7} and $BT_{MSG-1/2/3}$ exhibits a relatively high bias (−1.62 K on average) and is distinguishable from the other pairs of geostationary satellites, in contrast to its relatively high seasonal variations. The distribution of the decadal initial bias for all the geostationary platforms over the 2012–2016 period [Fig. 7(c)] reveals a multimodal distribution, which averages at 0.25 K and displays a standard deviation of 1.65 K. Fig. 7(b) shows that the corrections applied to the geostationary IR observations improve the error as well as the disparity of the scatter plot over the whole period and for all the geostationary platforms. These results are confirmed by the Gaussian distribution of the decadal bias for corrected BT_{GEOS} shown in Fig. 7(c), which averages at 0.19 K with a standard deviation of 0.87 K. The resulting geostationary satellite calibration residuals specifications are hence well within the 1 K limit previously mentioned and demonstrate the importance to develop a correction procedure for the geostationary IR observations at cold temperatures.

D. Limb-Darkening Adjustment

1) Methodological Considerations: To complete the homogenization procedure of the geostationary database, we focus now on the dependence of the BT_{GEOS} on the VZA. This issue, also called limb darkening, corresponds to a decrease in the temperature as the VZA increases. The greater optical path length of the absorbing atmosphere, as the VZA increases, results in a larger atmospheric absorption. Indeed, a longer optical path length contains much more water vapor and ozone explaining the observation of colder temperatures [35], [37], [38]. Cloudy scenes imply a second mechanism in the VZA issues [35]. A geometric effect may also be involved when the sides of the clouds obstruct the Earth's emitted radiation at a large VZA. Some studies on these geometric effects discussed the different configurations of cloud fields [39]. To prevent an erroneous analysis between meteorological situations, which occurred at nadir and at a large VZA, the BTs have to be limb-adjusted. Some studies have been carried out to limb adjust the IR observations for cloudy regions by establishing empirical limb correction functions, depending on the cosine of zenith angle from the radiative transfer model for low earth orbit platforms [39] and IR geostationary observations [40]. However, it has been shown [41] that the corrections developed by [39] underestimate the observed BTs. The variation of the radiance, according to the zenith angle, is approximated in the CLAUS data set, by applying a function of the cosine of the zenith angle. Another way to face the limb-darkening issues is to use observations from low earth orbit platforms. Limb-correction algorithms have been developed for microwave observations from the AMSU-A and are based on a physical-statistical methodology [37]. The limb-darkening problem has also been

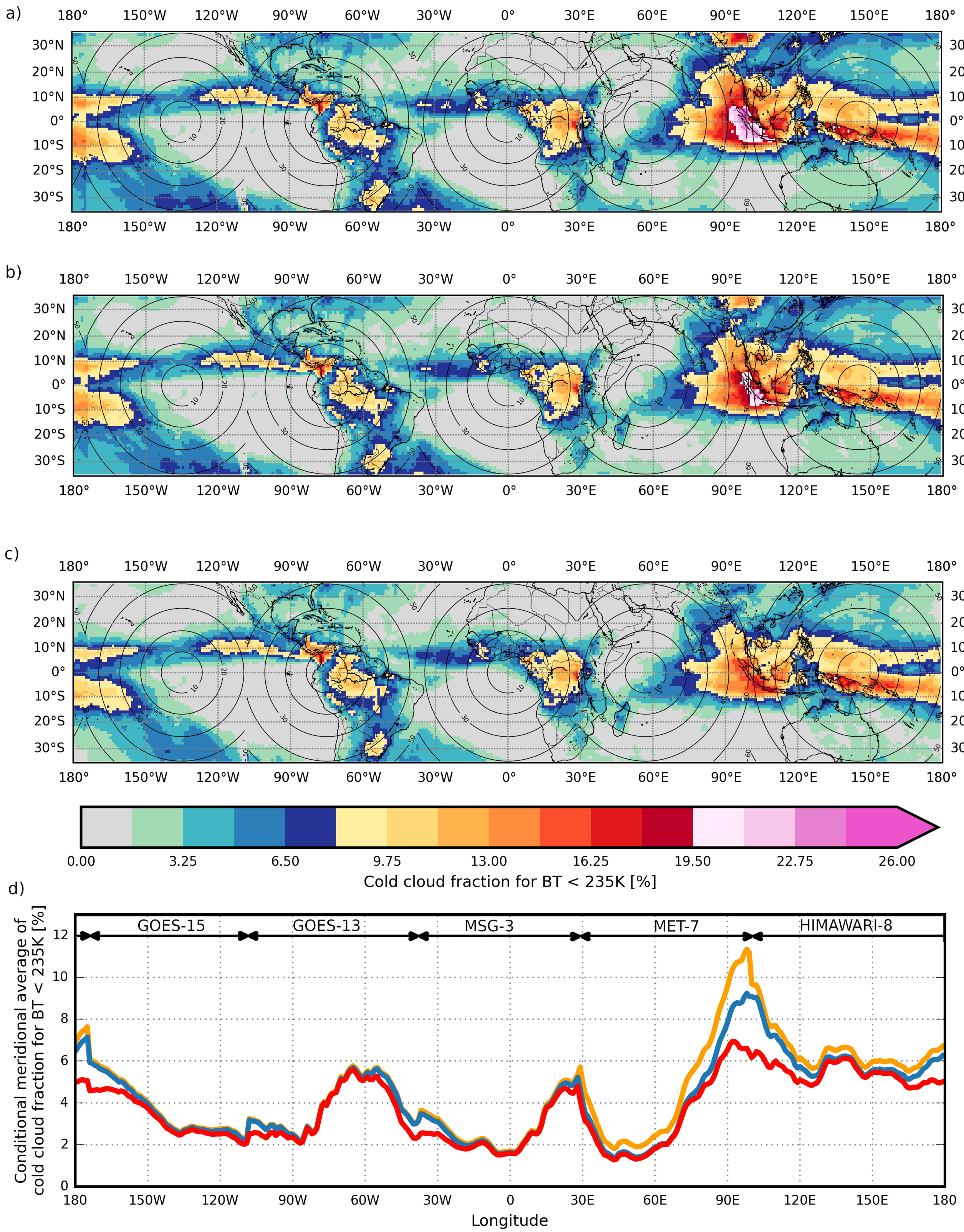

Fig. 10. Map of the mean cold cloud fraction (%) for BT_{GEO} < 235 K over 2016 (a) by using the initial BT_{GEO} before any corrections, (b) by using the calibrated and spectrally corrected BT_{GEO}, and (c) after applying the VZA corrections on BT_{GEO}. The black circles represent the different levels of VZA. (d) Conditional meridional average of the cold cloud fraction for BT_{GEO} < 235 K before any corrections (orange line), after applying the calibration and spectral corrections (blue line) and after applying the VZA corrections (red line).

explored by comparing the radiances from the geostationary platforms with observations from polar orbiter platforms [40]. Some limb-darkening corrections have been computed from collocated pairs of GOES platforms (GOES-8/GOES-10) and Meteosat platforms (Meteosat-5/Meteosat-7) [35]. They proposed a two-step correction. First, a correction table of the BT_{GEO} as a function of VZA is applied to BT_{GEO} only for observations in the tropics. For mid-latitude regions, an additional correction is applied to tackle the latitudinal and seasonal dependence of BT_{GEO}. This dependence is explained by a smaller contrast between the cloud top and the Earth's surface in mid-latitudes than over the tropics. This limb-darkening correction is used in GridSat and ISCCP data sets [4]. However, this methodology is likely to suffer from limitations to be used to homogeneously limb adjust a fleet of geostationary satellites. Indeed, the limb adjustment, developed in the 2000s and empirically derived from a combination of a specific and limited set of instruments, may also be biased for other and new generation of geostationary instruments [12]. Moreover, the computation of the limb-darkening correction is limited by the range of VZA, due to the combination of the fixed location of geostationary satellites inducing few observations of cold BT_{GEO}.

It appears important, for this article, to tackle limb-darkening issues on geostationary satellite per geostationary satellite over the full time period by using a common reference, such as the IR observation from the ScaRaB instrument. This correction focuses on cold clouds monitored by the IR imagery of geostationary satellites previously intercalibrated and normalized into a 10.5–12.5 μm IR equivalent BT, called BT^{*}_{GEO}. For this purpose, we perform for each GEO platform a collocation procedure between the regular lon/lat 0.5° and corrected IR geostationary data, presented previously, and the ScaRaB/L2B IR observation over the entire 2012–2016 period. The collocation procedure is applied under some criteria. Where the zenithal angles of ScaRaB do not exceed 20°, the geostationary zenith angles can range from 0° to 70°. The collocation is also performed with a time delay of less than 10 min between the GEO and the ScaRaB observations and for BT_{ScaRaB}, which does not exceed 235 K for standard deviations lower than 2 K.

GEO-ScaRaB match-ups are binned into geostationary zenith angle intervals of 2° and for zenith angles ranging from 20° to 70°. For GEO VZAs lower than 20°, a unique limb correction is performed. Moreover, to ensure a relevant sample size on each 2° zenith angle bin, the regressions are applied annually. For each zenith angle interval, the collocated $BT_{GEO}*$ and BT_{ScaRaB} are binned and averaged for every BT_{ScaRaB} interval of 5 K, from 180 to 235 K. To filter corrupted collocated points, the binning procedure is performed when at least ten samples are present. The limb correction then consists of applying annual regressions between the binned GEO and ScaRaB data for every 2° zenith angle bin and for each geostationary platform. A second-order polynomial regression has been preferred over the linear regression, due to slight improvements in the minimization of the residuals.

2) Results: Fig. 8(a)–(c) shows the variation of the initial bias between each GEO platform and ScaRaB, according to the VZA for different bins of ScaRaB temperatures and over the 2012–2016 period. First, one can observe a negative increase in the bias as the VZA increases, whatever the range of BT. For VZA lower than 30°, the absolute bias seems to be lower than 1 K, whatever the BT_{ScaRaB} is. However, we can observe drastic differences in the bias evolution depending on the BT_{ScaRaB} bin. Indeed, at warmer BT_{ScaRaB} [225–235 K], the negative increase in the bias according to the VZA is more pronounced than for colder values of BT_{ScaRaB} [190–200 K]. For a VZA at 40°, the bias averages at -0.63 K for BT_{ScaRaB}, ranging from 190 to 200 K and for all the GEO platforms, while the bias averages at -2.9 K for BT_{ScaRaB} greater than 225 K and for a similar VZA. It is also to be noticed that the disparity of the bias among GEO platforms increases with the VZA. Thus, at a 60° zenith angle and for the 225–235 K range, the bias varies from -7.4 to -9.5 K for GOES-15 and Meteosat-7, respectively. Such large errors have been previously reported for an older Meteosat first-generation satellite (Meteosat-4) compared to NOAA/AVHRR reference [27]. Note that the uncertainty does not increase much with the BT but increases with the VZA. Fig. 8(d)–(f) shows the results of the limb-darkening corrections according to the variation of the zenith angle for all the geostationary platforms and for different ranges of BT_{ScaRaB}. Over the whole range of ScaRaB BTs, the residual biases average at 0 K, regardless of the geostationary platform and the zenith angles. These results demonstrate the capability of the limb-darkening correction methodology we have developed. An independent validation is provided in Fig. 9 by comparing pairs of geostationary platform observations. It shows the variation of the decadal biases of $BT_{GEO}*$ between pairs of geostationary satellites, according to the difference of their VZAs (ΔVZA), before and after applying limb-darkening corrections. A ΔVZA of 0° means that two adjacent geostationary platforms observe the same region with an equivalent VZA. On the contrary, a large ΔVZA indicates that a given geostationary platform observes a region with a nadir zenith angle, while the adjacent geostationary platform monitors the same region with a limb zenith angle. Before applying the zenith angle corrections, we can observe an increase of $BT_{GEO}*$ bias for all the platforms from ~ -5 to ~ 5 K as the ΔVZA moves from $-50°$ to 40° [Fig. 9(a)]. The standard deviation, on its side, varies between 0.86 K for a low ΔVZA and 1.57 K for large ΔVZA. Results indeed indicate a larger disparity of the $BT_{GEO}*$ biases between pairs of geostationary satellites for large ΔVZA. After applying the zenith angle correction [Fig. 9(b)], the $BT_{GEO}**$ bias is relatively stable and averages at 0.09 K with a standard variation of 1.43 K, regardless of the variation of ΔVZA. The standard deviation varies from 1.05 to 1.78 K for low and large ΔVZA, respectively. Note that when the limb-darkening issue is clearly improved and corrected, the standard deviation for a low VZA is a little larger than before applying the VZA correction.

IV. Discussion and Conclusion

In summary, a level 1c IR GEOring data set is introduced. This data set is a consistent 10.5–12.5 μm IR equivalent BT data set, with a homogeneous recalibration, a 0.04° × 0.04° spatial resolution, a 30 min common time resolution, and a correction for limb effect. The data set covers the 2012–2016 period. The global homogeneity of the IR GEOring data set, regardless of the variation of VZA, is then characterized by a standard deviation of 1.43 K within any of two geostationary satellites.

As discussed in the Introduction section, global geostationary IR observations provide useful resources to carry out studies on convective systems. Cold cloud tracking algorithms usually delineate cold clusters by applying a 235 K threshold on IR geostationary data. To evaluate the impact of the geostationary IR data homogenization on high cold clouds, we compute the cold cloud fraction. The fraction is determined by applying a 235 K threshold on the initial BT_{GEO} before any corrections, on the spectrally adjusted and calibrated BT_{GEO} and finally on the VZA corrected IR data for the 2016 period and over the entire tropics. The computations are performed by using the selected configuration of the geostationary fleet and the map of cold cloud fraction provided on a $1^{\circ} \times 1^{\circ}$ grid [Fig. 10(a)–(c)]. Before corrections, a local maximum of cold cloud fraction reaching 26% is seen in the Meteosat-7 area over the west coast of the Indo–China peninsula. However, the calibration correction allows to attenuate this fraction which falls to 22%. Also, note that this region is observed by Meteosat-7 with a VZA of 47°. After the limb-adjustment procedure, the value of cold cloud fraction for this specific region decreases to 17%. The maximum of cold cloud fraction is now located over the warm pool and is observed by the HIMAWARI-8 platform. One can also see that the local maximum of cold cloud fraction over the Tibetan plateau is strongly attenuated with all the corrections. Before applying the homogenization procedure, one can observe some steps of the conditional meridional average of cold cloud cover at the boundary of Meteosat-7 and HIMAWARI-8 and between HIMAWARI-8 and GOES-15, reaching 1.65% and 1.47%, respectively [Fig. 10(d)]. The combined corrections improve these issues and show a cold cloud cover exhibiting a smoother transition from one platform to another. Fig. 10(d) shows similar cold cloud covers for low VZA between a unique calibration/spectral correction and the combined calibration/spectral and VZA corrections, while one can observe a decrease in cold cloud cover for large VZA between the two corrections.

The extension of the current database beyond 2016 is under consideration. The configuration of the fleet, nevertheless, drastically changes in 2017 with the end of operation of Meteosat-7 and the arrival of MSG-1 in February on a shifted position, although not fully covering the Indian Ocean. Tests are needed to explore the sensitivity of the database to this new configuration. The use of INSAT-3D is also contemplated as a better way to bridge MSG-1 and HIMAWARI-8 data. GOES-R has become operational and the stream of GOES-16 replaces GOES-13 in December 2017. Similarly, GOES-17 is now operational as the new GOES west coverage replacing the GOES-15 platform from February 2019.

Up to the end of 2018, the Megha-Tropiques mission has been operated nominally granting the possibility of extending the present effort up to that time. While the present work relies on the ScaRaB instrument onboard Megha-Tropiques, it can easily be applied to alternative IR reference observations, from hyperspectral sounders, for instance. This article indicates that the final calibrated and limb-adjusted IR observations for $BT < 240$ K can be homogeneous throughout the GEOring with less than 1.5 K standard deviation, and that further future efforts should strive for such, or better, accuracy.

Acknowledgment

The authors would like to thank the ESPRI/IPSL team for providing computing and storage resources. They also thank the DWD as well as the French data center AERIS for their help in accessing the data (GEOring, ScaRaB). They also thank G. Urbani and C. Bovalo for their help in handling the geostationary satellite data archive. They further acknowledge M. Dejus, Project Manager at CNES, and his team for their help on the technical aspects of ScaRaB. The ScaRab L2B is available in the ICARE data and service center with an *Anonymous* File Transfer Protocol (ftp://ftp.icare.univ-lille1.fr/SPACEBORNE/SCARAB/MT1_L2B-FLUX-SCASL1A2_0.5deg.v2.01/). The calibration coefficients and the limb-adjustment coefficients are available at the following DOI: https://doi.org/10.14768/20191125.

References

[1] R. A. Schiffer and W. B. Rossow, "The International Satellite Cloud Climatology Project (ISCCP): The first project of the World Climate Research Programme," *Bull. Amer. Meteorol. Soc.*, vol. 64, no. 7, pp. 779–784, Jul. 1983.

[2] M. L. Salby, H. H. Hendon, K. Woodberry, and K. Tanaka, "Analysis of global cloud imagery from multiple satellites," *Bull. Amer. Meteorol. Soc.*, vol. 72, no. 4, pp. 467–480, Apr. 1991.

[3] G. J. Huffman *et al.*, "The Global Precipitation Climatology Project (GPCP) combined precipitation dataset," *Bull. Amer. Meteorol. Soc.*, vol. 78, no. 1, pp. 5–20, 1997.

[4] K. R. Knapp *et al.*, "Globally Gridded Satellite observations for climate studies," *Bull. Amer. Meteorol. Soc.*, vol. 92, no. 7, pp. 893–907, Jul. 2011.

[5] R. A. Kohrs, M. A. Lazzara, J. O. Robaidek, D. A. Santek, and S. L. Knuth, "Global satellite composites—20 years of evolution," *Atmos. Res.*, vols. 135–136, pp. 8–34, Jan. 2014.

[6] P. Zhang, K. Holmlund, M. Goldberg, and J. Lafeuille, "The Global Space-based Inter-Calibration System (GSICS)," in *Proc. IEEE Int. Geosci. Remote Sens. Symp. (IGARSS)*, Jul. 2016, pp. 5522–5523.

[7] T. J. Hewison *et al.*, "GSICS inter-calibration of infrared channels of geostationary imagers using Metop/IASI," *IEEE Trans. Geosci. Remote Sens.*, vol. 51, no. 3, pp. 1160–1170, Mar. 2013.

[8] D. R. Doelling *et al.*, "Geostationary enhanced temporal interpolation for CERES flux products," *J. Atmos. Ocean. Technol.*, vol. 30, no. 6, pp. 1072–1090, Jun. 2013.

[9] T. J. Hewison and J. Muller, "Ice contamination of Meteosat/SEVIRI implied by intercalibration against Metop/IASI," *IEEE Trans. Geosci. Remote Sens.*, vol. 51, no. 3, pp. 1182–1186, Mar. 2013.

[10] B. Scarino, D. R. Doelling, C. Haney, K. Bedka, and P. Minnis, "Utilizing the precessing orbit of TRMM to produce hourly corrections of geostationary infrared imager data with the VIRS sensor," *Proc. SPIE*, vol. 10403, Aug. 2019, Art. no. 104030H.

[11] G. J. Robinson and K. I. Hodges, "Cloud archive user service user guide," Tech. Rep., 2005, p. 16. AQ:8

[12] K. R. Knapp, "Gridded satellite B1 FCDR—Monthly means," Tech. Rep., 2016.

[13] J. E. Janowiak, R. J. Joyce, and Y. Yarosh, "A real-time global half-hourly pixel-resolution infrared dataset and its applications," *Bull. Amer. Meteorol. Soc.*, vol. 82, no. 2, pp. 205–217, Feb. 2001.

[14] Y. Desormeaux, W. B. Rossow, C. L. Brest, and G. G. Campbell, "Normalization and calibration of geostationary satellite radiances for the International Satellite Cloud Climatology Project," *J. Atmos. Ocean. Technol.*, vol. 10, no. 3, pp. 304–325, Jun. 1993.

[15] T. Fiolleau and R. Roca, "An algorithm for the detection and tracking of tropical mesoscale convective systems using infrared images from geostationary satellite," *IEEE Trans. Geosci. Remote Sens.*, vol. 51, no. 7, pp. 4302–4315, Jul. 2013.

[16] M. Schröder, M. König, and J. Schmetz, "Deep convection observed by the Spinning Enhanced Visible and Infrared Imager on board Meteosat 8: Spatial distribution and temporal evolution over Africa in summer and winter 2006," *J. Geophys. Res.*, vol. 114, no. D5, pp. 1–14, 2009.

[17] B. E. Mapes and R. A. Houze, "Cloud clusters and superclusters over the oceanic warm pool," *Monthly Weather Rev.*, vol. 121, no. 5, pp. 1398–1416, May 1993.

[18] R. Roca *et al.*, "The Megha-Tropiques mission: A review after three years in orbit," *Frontiers Earth Sci.*, vol. 3, p. 17, May 2015.

[19] R. Kandel *et al.*, "The ScaRaB earth radiation budget dataset," Natural AQ:9 Resour. Canada/ESS/Sci. Tech. Publishing Services, Tech. Rep., 1998.

[20] J.-P. Duvel *et al.*, "The ScaRaB-Resurs Earth radiation budget dataset and first results," *Bull. Amer. Meteorol. Soc.*, vol. 82, no. 7, pp. 1397–1408, Jul. 2001.

[21] M. Viollier and P. Raberanto, "Radiometric and spectral characteristics of the ScaRaB-3 instrument on Megha-Tropiques: Comparisons with ERBE, CERES, and GERB," *J. Atmos. Ocean. Technol.*, vol. 27, no. 3, pp. 428–442, Mar. 2010.

[22] A. Rosak, T. Tremas, N. Karouche, L. Gillot, and O. Simonella, "Radiometric and geometric Scarab-Megha-Tropiques ground calibration comparison with first in orbit calibration," in *Proc. IEEE Int. Geosci. Remote Sens. Symp.*, Jul. 2012, pp. 4746–4749.

[23] N. Karouche, C. Goldstein, A. Rosak, C. Malassingne, and G. Raju, "MEGHA-TROPIQUES satellite mission: In flight performances results," in *Proc. IEEE Int. Geosci. Remote Sens. Symp.*, Jul. 2012, pp. 4684–4687.

[24] T. L. Trémas, N. Karouche, A. Rosak, A. Meygret, O. Aznay, and E. Hillairet, "ScaRaB: First results of the scanner for radiative budget on board the Indo-French satellite Megha-Tropiques," *Proc. SPIE*, vol. 8510, Oct. 2012, Art. no. 851002.

[25] R. Roca *et al.*, "Le bilan scientifique de la mission Megha-Tropiques AQ:10 après 8 ans dans l'espace," *La Météorologie*, no. 107, p. 36, 2019.

[26] J. P. Duvel and P. Raberanto, "A geophysical cross-calibration approach for broadband channels: Application to the ScaRaB experiment," *J. Atmos. Ocean. Technol.*, vol. 17, no. 12, pp. 1609–1617, Dec. 2000.

[27] D. R. Doelling, D. Morstad, B. R. Scarino, R. Bhatt, and A. Gopalan, "The characterization of deep convective clouds as an invariant calibration target and as a visible calibration technique," *IEEE Trans. Geosci. Remote Sens.*, vol. 51, no. 3, pp. 1147–1159, Mar. 2013.

[28] G. L. Smith, Z. P. Szewczyk, K. J. Priestley, and R. Roca, "Method of comparing CERES and ScaRaB 3 measurements," in *Proc. Sensors, Syst., Next-Gener. Satellites XVI SPIE*, 2012, pp. 7193–7196.

[29] T. L. Trémas, O. Aznay, and O. Chomette, "ScaRaB and CERES-Terra: Results of the inter-comparison campaigns," *Proc. SPIE*, vol. 9973, Sep. 2016, Art. no. 99730B.

[30] N. Gif, O. Chomette, and P. Raberanto, "Co-location algorithms geophysical data projection using pixel point spread function," Megha-AQ:11 Tropiques Tech. Memo. 2, 2011.

[31] M. Capderou, "Sampling. Comparison with other Meteorological Satellites," Megha-Tropiques Tech. Memo. 1, 2009.

[32] C. L. Brest, W. B. Rossow, and M. D. Roiter, "Update of radiance calibrations for ISCCP," *J. Atmos. Ocean. Technol.*, vol. 14, no. 5, pp. 1091–1109, Oct. 1997.

[33] K. R. Knapp, "Calibration assessment of ISCCP geostationary infrared observations using HIRS," *J. Atmos. Ocean. Technol.*, vol. 25, no. 2, pp. 183–195, Feb. 2008.

[34] M. König, J. Schmetz, and S. Tjemkes, "Satellite intercalibration of IR window radiance observations," *Adv. Space Res.*, vol. 23, no. 8, pp. 1341–1348, Jan. 1999.

[35] R. Joyce, J. Janowiak, and G. Huffman, "Latitudinally and seasonally dependent zenith-angle corrections for geostationary satellite IR brightness temperatures," *J. Appl. Meteorol.*, vol. 40, no. 4, pp. 689–703, Apr. 2001.

[36] T. H. von der Haar and S. Q. Kidder, *Satellite Meteorology—An Introduction*. New York, NY, USA: Academic, 1995.

[37] M. D. Goldberg, D. S. Crosby, and L. Zhou, "The limb adjustment of AMSU—A observations: Methodology and validation," *J. Appl. Meteorol.*, vol. 40, no. 1, pp. 70–83, Jan. 2001.

[38] Q. Liu and F. Weng, "Uses of *NOAA-16* and *-18* satellite measurements for verifying the limb-correction algorithm," *J. Appl. Meteorol. Climatol.*, vol. 46, no. 4, pp. 544–548, Apr. 2007.

[39] P. Minnis, "Viewing zenith angle dependence of cloudiness determined from coincident GOES east and GOES west data," *J. Geophys. Res.*, vol. 94, no. D2, pp. 2303–2320, 1989.

[40] N. J. Elmer, E. Berndt, and G. J. Jedlovec, "Limb correction of MODIS and VIIRS infrared channels for the improved interpretation of RGB composites," *J. Atmos. Ocean. Technol.*, vol. 33, no. 5, pp. 1073–1087, May 2016.

[41] K. I. Hodges, D. W. Chappell, G. J. Robinson, and G. Yang, "An improved algorithm for generating global window brightness temperatures from multiple satellite infrared imagery," *J. Atmos. Ocean. Technol.*, vol. 17, no. 10, pp. 1296–1312, Oct. 2000.

Thomas Fiolleau received the Ph.D. degree from Ecole Polytechnique, Paris, France, in 2010 with a thesis on the use of satellite observation to study mesoscale convective systems in the framework of the Megha-Tropiques Indo–French Satellite Mission.

He was an Associate Engineer with the Laboratoire de Météorologie Dynamique (LMD), Paris, for two years. He worked as a United Nations Educational, Scientific and Cultural Organization (UNESCO) Consultant with the Centro Nacional de Monitoramento e Alertas de Desastres Naturais (CEMADEN), Brazil, a Brazilian operational center, where he worked on the development of operational algorithms to forecast convective systems. After two years at CNRM (joint laboratory between CNRS and Météo-France), he joined the CNRS in 2016 as a Research Engineer with the Laboratoire d'Etudes en Géographie et Océanographie Spatiales, Toulouse, France. His areas of specialization are remote sensing, image processing, tropical climate and meteorology, and his researches interests are focused on the development of cloud tracking algorithms from geostationary satellites and the study of the life cycle of tropical mesoscale convective systems by using satellite observations.

Rémy Roca received the M.S. degree in fundamental physics, with major in remote sensing, and the Ph.D. degree in 2000 from Université Paris, Paris, France, with a thesis on the use of satellite observations to evaluate climate models. AQ:12

He was with the Scripps Institution of Oceanography, University of California, San Diego, CA, USA, for almost two years where he got familiar with image processing and cloud detection and tracking algorithms from geostationary satellites. From 2001 to 2012, he was with the Laboratoire de Météorologie Dynamique, Institut Pierre et Simon Laplace, Paris, where he was a CNRS Researcher. He was appointed a Mission Scientist of the Megha-Tropiques Indo–French Satellite Mission and took over the PIship of the mission in 2007. He is a Senior CNRS Researcher with the Laboratoire d'Etudes en Géographie et Océanographie Spatiales, Toulouse, France. His broad interests are focused on the study of the water cycle in the tropics and the use of satellite observations to investigate the tropical variability. He has more than 15 years of experience in the field of tropical climate, meteorology, and remote sensing.

Dr. Roca was the Chairman of the International Precipitation Group in 2014 and 2015, and since 2016, he has been co-leading the GEWEX/WCRP Data Analysis Panel.

Sophie Cloché received the M.S. degree in fundamental physics, with a specialization in remote sensing, and the Ph.D. degree in 1996 with a thesis on the use of satellite observations (POLDER) for cloud and water vapor detection from Université Paris, Paris, France. AQ:13

From 1996 to 1998, she was a Post-Doctoral Position with the Laboratoire de Météorologie Dynamique (LMD/CNRS), Paris, working on narrow to broadband conversion to estimate the radiative fluxes. From 1998 to 2001, she was as a Research Engineer, on database management for the INDOEX program, LMD. In 2001, she obtained a fix position with the CNRS, Institut Pierre-Simon Laplace (IPSL), Paris, as Research Engineer, and also involved in database management for different national and international projects (AMMA, Hymex, GEWEX-Cloud Assessment for example). She is the Co-ordinator of the scientific ground segment for the Megha-Tropiques mission and involved in the CM SAF from Eumetsat for the development of a global precipitation product. She also coordinates space activities at IPSL and she is responsible of the database management of observations at IPSL.

Dominique Bouniol received the Ph.D. degree from the University of Paris, Paris, France, in 2000, with a thesis on process-oriented use of observational data sets for understanding mesoscale storm deepening.

After 18 months in the Radar Meteorology Group, University of Reading, Reading, England, she joined AQ:14 the CNRS as a Researcher in 2002, first in CETP where she was involved in the implementation and exploitation of ground-based cloud radar in the framework of the Cloudnet project. She led the deployment of the airborne version of the cloud radar within the AMMA experiment in Niger and Senegal, in 2006. While she was with CNRS, she joined the CNRM (joint laboratory between CNRS and Météo-France), in 2006, where her research focuses on physical processes involved in the tropical mesoscale convective system life cycle and more generally on tropical cloud processes using both observations and modeling tools.

Patrick Raberanto received the Ph.D. degree in astronomy and space technology from Paul Sabatier University, Toulouse, France, in 1984.

In 1990, he joined the Laboratoire de Météorologie Dynamique (LMD), Ecole Polytechnique, Paris, as a CNRS Research Engineer and was implied in the ScaRaB project. In the framework of the Megha-Tropiques mission, he was in charge of the ScaRaB calibration, validation, and the development of the ScaRaB level-2 products. His research interests include radiometric calibration and radiative budget observation.

AUTHOR QUERIES

AUTHOR PLEASE ANSWER ALL QUERIES

PLEASE NOTE: We cannot accept new source files as corrections for your article. If possible, please annotate the PDF proof we have sent you with your corrections and upload it via the Author Gateway. Alternatively, you may send us your corrections in list format. You may also upload revised graphics via the Author Gateway.

1) **Please be aware that authors are required to pay overlength page charges ($230 per page) if the article is longer than 6 pages. If you cannot pay any or all of these charges please let us know. GRS Society members receive a discounted rate of $200 per page.**
2) **This pdf contains 2 proofs. The first half is the version that will appear on Xplore. The second half is the version that will appear in print. If you have any figures to print in color, they will be in color in both proofs.**
3) **The "Open Access" option for your article expires when the article is published on Xplore in an issue with page numbers. Articles in "Early Access" may be changed to Open Access. If you have not completed your electronic copyright form (ECF) and payment option please return to Scholar One "Transfer Center." In the Transfer Center you will click on "Manuscripts with Decisions" link. You will see your article details and under the "Actions" column click "Transfer Copyright." From the ECF it will direct you to the payment portal to select your payment options and then return to ECF for copyright submission.**

AQ:1 = Please note that "viewing zenithal angle" has been changed to "viewing zenith angle" throughout the text for consistency.

AQ:2 = Please confirm or add details for any funding or financial support for the research of this article.

AQ:3 = Please confirm whether the edits made in the current affiliation of all the authors are correct.

AQ:4 = Please confirm the postal code for CNRS, Institut Pierre Simon Laplace, Université de Toulouse, and Laboratoire de Météorologie Dynamique.

AQ:5 = Please provide the expansions for SEVIRI and AMSU.

AQ:6 = Please check the sentence "The use of geophysical targets like …" for clarity.

AQ:7 = Please check and confirm whether the edits made are appropriate: "Some studies on these geometric effects discussed the different configurations of cloud fields."

AQ:8 = Please provide the organization name, organization location, and report no. for Refs. [11] and [12].

AQ:9 = Please provide the organization location and report no. for Ref. [19].

AQ:10 = Please provide the volume no. for Ref. [25].

AQ:11 = Please provide the organization name and organization location for Refs. [30] and [31].

AQ:12 = Please provide the year of completion when the author Rémy Roca received the M.S. degree.

AQ:13 = Please provide the year of completion when the author Sophie Cloché received the M.S. degree.

AQ:14 = Please provide the location for CETP.

Homogenization of Geostationary Infrared Imager Channels for Cold Cloud Studies Using Megha-Tropiques/ScaRaB

Thomas Fiolleau, Rémy Roca, Sophie Cloché, Dominique Bouniol, and Patrick Raberanto

***Abstract*— Infrared (IR) observations from the fleet of multiagencies meteorological geostationary satellites have a great potential to support scientific and operational investigations at a quasi-global scale. In particular, such a data record, defined as the GEOring data set, is well suited to document the tropical convective systems life cycles by applying cloud tracking algorithms. Yet, this GEOring data set is far from being homogeneous, preventing the realization of its potential. A number of sources of inhomogeneities are identified ranging from spatiotemporal resolutions to spectral characteristics of the IR channels and calibration methodologies. While previous efforts have attempted to correct such issues, the adjustment of the cold part of the IR spectrum remains unfit for cold cloud studies. Here, a processing method is introduced to minimize the inhomogeneities against a reference observational data set from the Scanner for Radiation Budget (ScaRaB) instrument onboard the Megha-Tropiques satellite. The method relies on the collocations between the geostationary observations and the reference. The techniques exhibit significant sensitivity to the selection of the relevant pairs of observations requiring a dedicated filtering of the data. A second effort is then proposed to account for the limb-darkening effect and a method is developed to correct the brightness temperature (BT) dependence** AQ:1 **on the geostationary viewing zenith angle (VZA). Overall, results show a residual after the processing of 0 K between any of the geostationary data and the ScaRaB reference. The final calibrated and limb-adjusted IR observations are then homogeneous for cold BT lower than 240 K with a standard deviation lower than 1.5 K throughout the GEOring.**

***Index Terms*— Calibration and spectral corrections, cold cloud studies, geostationary satellites, infrared (IR) image sensors, limb-darkening corrections.**

I. Introduction

METEOROLOGY agencies monitor individually operational geostationary platforms, which when used all together permit an observation for all longitudes of the Earth on a large latitudinal band (~60° S–60° N) with similar instruments. The potential benefit of such an observing capability has triggered numerous efforts in the past 40 years to make use of it for various applications, ranging from the elaboration of a unique perspective on clouds studies [1], [2] for precipitation estimation [3], climate studies [4], and global visualization applications [5]. Yet, when carefully examined, this GEOring appears to be far from a homogenous suite of instruments operated in a similar fashion. The space/time resolution and sampling differ across the platforms. The acquisition procedure also differs among the satellites (from South to North, North to South, or by sector). The calibration procedure of each instrument is also performed at the individual level with the instruments' specific modes of operation. Since 2011, for the infrared (IR) channels, the agencies provide alternative calibration coefficients obtained from a statistical comparison to hyperspectral IR measurements from low earth-orbiting satellites using the common methodology of the Global Space-Based InterCalibration System (GSICS) [6]. Nevertheless, the GSICS currently only provides calibration coefficients referenced to the NASA Earth Observing System (EOS), Aqua Atmospheric IR Sounder (AIRS), and the Exploitation of Meteorological Satellites (EUMETSAT)–Centre National d'Etudes Spatiales (CNES), Meteorological Operation (MetOp), and IR Atmospheric Sounding Interferometer (IASI) calibration standard. This harmonization effort does not take into account spectral band responses and viewing angle effects, which are needed for sensor homogenization. Indeed, while often referred to as a unique IR channel, the multiple instruments do show some spectral differences as well.

Most of the spectral imagers onboard geostationary satellites monitor with a relatively high temporal frequency the calibration coefficients for thermal IR channels by using onboard blackbody references. Some of the differences in the temperature measurements from one geostationary satellite to another can be explained by the differences in the calibration references, methods, as well as in the spectral filter functions. Moreover, it has been observed that the spectral imagers may degrade over time with different rates [7], [8]. The geostationary imagers can also be affected by short-term variations. The accumulation of ice on the surface of the imager optics modifies their spectral response function (SRF) and consequently affects the measurement of the temperatures. To face these issues, decontamination events are regularly applied to the radiometers inducing

AQ:2 Manuscript received July 17, 2019; revised November 25, 2019 and January 22, 2020; accepted February 4, 2020. *(Corresponding author: Thomas Fiolleau.)*

AQ:3 Thomas Fiolleau and Rémy Roca are with the Laboratoire d'Etudes en Géophysique et Océanographie Spatiales, CNRS, 31400 Toulouse, France (e-mail: thomas.fiolleau@legos.obs-mip.fr; remy.roca@legos.obs-mip.fr).

Sophie Cloché is with CNRS, Institut Pierre Simon Laplace, 75252 Paris, France (e-mail: sophie.bouffies-cloche@ipsl.fr).

Dominique Bouniol is with the Centre National de Recherches AQ:4 Météorologiques, CNRS, Météo-France, Université de Toulouse, 31057 Toulouse, France (e-mail: dominique.bouniol@meteo.fr).

Patrick Raberanto is with the Laboratoire de Météorologie Dynamique, CNRS, 75016 Paris, France (e-mail: patrick.raberanto@lmd.polytechnique.fr).

Color versions of one or more of the figures in this article are available online at http://ieeexplore.ieee.org.

Digital Object Identifier 10.1109/TGRS.2020.2978171

TABLE I
SUMMARY OF THE TECHNICAL CHARACTERISTICS OF THE VARIOUS EXISTING IR GEORING DATA SETS

Products	Spatial resolution	Temporal resolution	Spatial coverage	Temporal coverage	Calibration and temporal normalization	Limb darkening correction	Data source
Gridsat-B1	0.07°	180 min	70°S-70°N	1980-present	HIRS channel 8 [14]	Yes	ISCCP-B1
CPC	~ 0.04°	30 min	60°S-60°N	2000–present	No absolute calibration and no temporal normalization	Yes	Native
CLAUS	0.5°	180 min	Global*	1983-2006	ISCCP- B3	Yes	ISCCP-B3
CLAUS	0.3°	180 min	Global*	1985–2008	ISCCP- B3	Yes	ISCCP-B3
ISCCP-B1	Native FoV subsampled to ~ 0.1°	180 min	70°S-70°N	1980-present	AVHRR channel 5 [13]	No	Native
ISCCP-B3	Native FoV subsampled to ~ 0.3°	180 min	70°S-70°N	1983-2009	AVHRR channel 5 [13]	No	Native
This study	0.04°	30 min	35°S-35°N	2012-2016	SCARAB-IR channel 4	yes	Native

instability in the temperature measurements [9]. This effect has been particularly shown for the Meteosat Visible IR Imager (MVIRI) onboard the Meteosat-7 geostationary platform.

A diurnal cycle effect can also affect the imager calibration, especially for the instruments on the three-axis stabilized geostationary platforms [7], [9]. It has been shown that the sun-synchronous orbits of MetOp/IASI and EOS/AIRS used in the GSICS calibration are not sufficient to completely correct the diurnal IR calibration issues [10]. The precessing orbit of the tropical rainfall measuring mission (TRMM) platform and the observations of its visible and IR scanner (VIRS) have then been used to quantify and correct such a midnight IR calibration anomaly [10]. IR observations are also dependent on the geostationary viewing zenith angle (VZA). The issue is called limb darkening, corresponding to a decrease in the temperature as the VZA increases.

These multiple sources of inhomogeneity have prevented the full use of this unique observational capability, although a number of successful projects have attempted to overcome the above-listed limitations. Indeed, a number of significant efforts have been proposed in the last two decades to produce more or less homogeneous "global" archive of geostationary data sets for various applications. It ranges from cloud climatology computations (International Satellite Cloud Climatology Project (ISCCP)-B1, ISCCP-B3, and Cloud Archive User Service (CLAUS) [11]), hurricane trend analysis, support of precipitation estimation (Gridded Satellite (GridSat) [12]), real-time monitoring of precipitation (Climate Prediction Center (CPC) [13]), for the enhancement of radiation budget averages [8]. Additional information on these GEOring data sets is listed in [4]. Table I summarizes the available IR GEOring data sets altogether with their respective properties and homogeneity levels. The ISCCP-B1 and B3 have been subsampled to a 180-min temporal resolution and to, respectively, ∼0.1° and ∼0.3° spatial resolution. They have been calibrated and spectrally normalized using advanced very high-resolution radiometer (AVHRR) observations [14]. The CLAUS data sets rely on the ISCCP-B3 and have been reprojected to an equal angle map projection with a spatial resolution of 0.3° and 0.5°. The GridSat-B1 is based on the ISCCP-B1 data set remapped to a 0.07° regular grid. In addition to the intercalibration used for the ISCCP data set, a second calibration using the high-resolution IR radiation sounder (HIRS) observations has been applied to correct a bias at cold temperatures observed after 2001. The CPC product is built in real time from native geostationary observations. The data are remapped to a regular grid of ∼0.04° spatial resolution and are available every 30 min. To reduce the spectral differences and calibration issues, a complex, multistep, multiregional procedure is applied by comparing the brightness temperatures (BTs) from pairs of geostationary platforms. However, this procedure does not provide any absolute calibration. Also note that a limb correction has been performed on the GridSat-B1, CPC, and CLAUS data. In short, while a number of efforts have paved the way for a quantitative use of the GEOring data sets, no dedicated effort toward the cold BT regimes has been promoted so far. Yet, cold cloud studies benefit a lot from geostationary IR observations, for cloud microphysical or macrophysical parameters retrievals. The spatiotemporal resolution of the measurements further allows the life cycle analysis of the cold cloudiness and the estimation of related parameters. The present GEOring attempt is directed toward these scientific applications. In particular, it will serve as the input of the realization of a tropical mesoscale convective system data set using the TOOCAN algorithm [15].

TABLE II
TECHNICAL CHARACTERISTICS OF THE OPERATIONAL GEOSTATIONARY SATELLITES FLEET AND THE ASSOCIATED IMAGERS USED OVER THE 2012–2016 PERIOD

Platform	Nadir location	Instrument	Central wavelength	Spectral interval	Spatial resolution at nadir	Temporal resolution	Region of interest	Source	Period
GOES-15	135° W	IMAGER	10.7 µm	10.2-11.2 µm	4 km	30 min	180° W-105° W 35° S-35° N	NOAA / DWD	Jan 2012-Dec 2016
GOES-13	75° W	IMAGER	10.7 µm	10.2-11.2 µm	4 km	30 min	111° W-30° W 35° S-35° N	NOAA / DWD	Jan 2012-Dec 2016
METEOSAT-8/9/10	0°	SEVIRI	10.8 µm	9.8-11.8 µm	3 km	15 min	45° W-45° E 35° S-35° N	EUMETSAT/ AERIS	Jan 2012-Dec 2016
METEOSAT-7 (IODC)	57.5° E	MVIRI	11.5µm	10.5-12.5 µm	5 km	30 min	12° E-107° E 35° S-35° N	EUMETSAT/ AERIS	Jan 2012-Dec 2016
MTSAT-2	145° E	IMAGER	10.8 µm	10.3-11.3 µm	4 km	30 min	94° E-170° W 35° S-35° N	AERIS/ CIMSS	Jan 2012-May 2015
HIMAWARI-8	140.7° E	AHI	11.2 µm	11.0-11.4 µm	2 km	10 min	94° E-170° W 35° S-35° N	AERIS/ JMA	Jun 2015-Dec 2016

Such analyses require observations with a minimal temporal resolution of 30 min [15], [16] to ensure tracked objects overlap between two images. Such kind of studies requires the use of thresholds applied to BT, ranging from 200 to 240 K, depending upon the analysis [17], [15]. A homogeneous data set is then mandatory, if one wants to proceed with the whole tropical belt. The homogeneity and basic requirements for a GEOring IR data set geared toward tropical cold cloud tracking applications can be summarized as follows:

1) High-resolution spatial footprint and high spatial resolution (∼5 km).
2) A minimum of 30 min time sampling.
3) A spatial coverage dedicated to the tropics.
4) Homogenized BTs through spectral and calibration adjustment.
5) Limb adjustment of IR observations.

Matching these requirements with the specifications of the IR data sets summarized in Table I confirms the need for a dedicated level 1c GEOring IR tailored for cold cloud tracking applications. Moreover, the current implementation of the GSICS coefficients computation is directed toward the warm part of the spectrum [8], ruling out its use for cold cloud studies calling for an alternative, cold cloud compliant, absolute calibration reference for the GEOring. The limb effect is less strong over the cold part of the temperature spectrum than at the warm and clear sky end of the spectrum, and the limb correction is easier to set up for cold cloudy scenes (BTs < 240 K) than for the clear atmosphere. This effect is strongly nonlinear and is thought to be impactful only for the viewing angle above 26.5° [11]; it may still require a correction for a homogeneous interpretation of the BT field all through the image. It is difficult to establish requirements once and for all in terms of residuals difference in the homogeneous data, based on the radiometric noise of the first generation sensors and the various sources of uncertainties in the adjustment procedure and basic cloud-oriented retrievals sensitivity. We propose to target a less than 1.5 K standard deviation among any of the two geostationary satellites in the final calibrated and limb-adjusted product for BTs < 240 K.

II. DATA

A. Five-Year Database of IR Geostationary Observations Over the Entire Tropics

Thermal channel BT images obtained by the operational meteorological geostationary satellite fleet are used over the 35°S–35°N latitude belt and for the whole 2012–2016 period. Table II shows the geostationary IR data used to cover the entire tropics for this period. The geostationary data set has been collected from different sources: the U.S. National Oceanic and Atmospheric Administration (NOAA), the European Organization for the Exploitation of Meteorological Satellites (EUMETSAT), the Japan Meteorological Agency (JMA), and the French Atmosphere and Service Data Pole (AERIS). Note that the Multifunctional Transport Satellite (MTSAT) data set has also been completed from the Space Science and Engineering Center (SSEC) of the University of

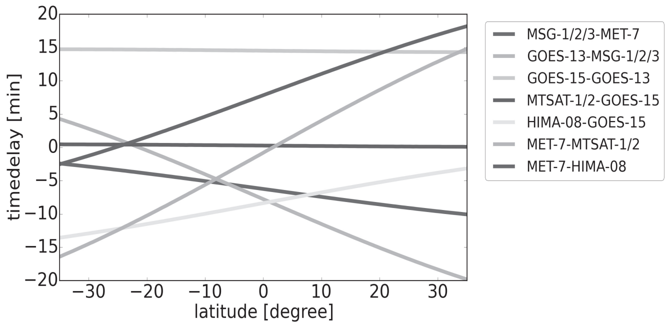

Fig. 1. Time delay of acquisition between pairs of geostationary images according to the latitude.

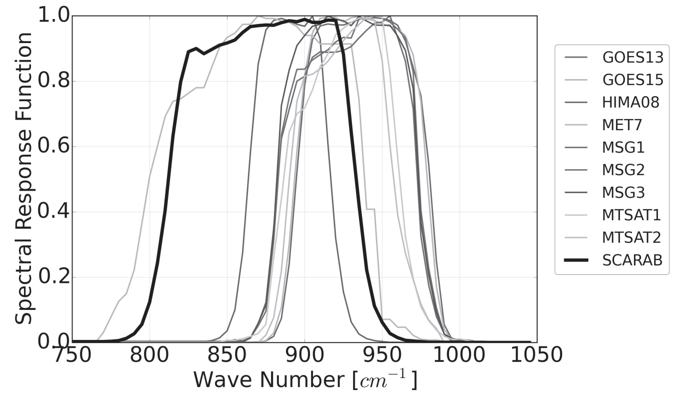

Fig. 2. SRF of the IR channel of the GEOring. The black line is the spectral response of the channel 4 of the ScaRaB instrument.

Wisconsin–Madison. The technical characteristics of each geostationary platform and their imagers are described in Table II and can differ from one platform to another. First, considering the temporal resolution, Meteosat Second Generation (MSG) and HIMAWARI-8 observe the Earth, respectively, with a 15- and 10-min time resolution, while the other platforms display a 30-min temporal resolution. Similarly, the scantimes vary from 7 min for HIMAWARI-8 to 25 min for Meteosat-7. The Geostationary Operational Environmental Satellite (GOES)-13 and GOES-15 sensors follow a complex scanning sector schedule. The full disk images are produced every 3 h, while the northern hemisphere and the southern hemisphere images are produced every 30 min with a time lag of few minutes between each scan. Also, note that the scanning schedule of MTSAT-2 does not provide half-hourly sampling of the southern hemisphere region. Contrary to the other imagers, the GOES-13 imager starts its earth scan at 15 and 45 min of the hour. Also note that Meteosat first- and second-generation imagers start their earth scan from the southeast corner, whereas NOAA and JMA platforms begin their earth scan from the northwest corner. All these temporal scanning differences imply some time delays between neighboring platforms observing the same region (Fig. 1). While the 15-min time delay is constant for the pairs of the GOES-15/GOES-13 and MTSAT-2/GOES-15 platforms, the time delay varies according to the latitude for the other pairs of geostationary platforms. At 35° S, a maximum time delay is found for the pair of MSG/GOES-13 platform of around 20 min. The maximum time delay amplitude accounted for the pair of the Meteosat-7/MTSAT-2 platforms and varies between −16 and 15 min.

Depending on the considered satellite, spatial resolution at nadir differs from one geostationary satellite to another and ranges from 2 km for HIMAWARI-8 to 5 km for Meteosat-7. In addition to the resolutions disparities, the GEOring is also characterized by differences in the central wavelength and the associated SRFs of each of the instruments (Fig. 2). While the central wavelength ranges between 10.7 and 11.5 μm for the GOES imagers and the Meteosat-7 imager, respectively, two types of SRFs can define the IR channels. The GOES-13, GOES-15, MTSAT-2, and HIMAWARI-8 imagers display narrowband channels with a bandwidth lower than 1 μm, whereas AQ:5 the Meteosat-7/MVIRI and MSG/SEVIRI imagers exhibit broader channels characterized by a 2 μm bandwidth. A broadband channel is highly sensitive to ice contamination on the optics of the imagers, modifying their SRFs, and consequently, introducing a calibration error. Operational decontamination procedures are applied regularly to remove the ice build-up on the optics. Thus, spectral differences, as well as the individual satellite calibration procedures, contribute to the GEOring radiometric inhomogeneities.

B. Megha-Tropiques/ScaRaB-3 Observations

The Scanner for Radiation Budget (ScaRaB) instrument on the Megha-Tropiques platform [18] is the third of its kind [19], [20] and has been designed to measure the Earth radiation components at the top of the atmosphere with high accuracy (<1%). The instrument acquires data across the satellite track with a swath of ∼2200 km from 30° S to 30° N. It is a broadband radiometer with four channels. The total channel measures the total energy between 0.2 and 100 μm. The shortwave channel (0.2–4 μm) is subtracted from the total channel to obtain the longwave part of the spectrum [21]. The fourth channel is an IR thermal channel (10.5–12.5 μm) which is used in this article (Fig. 2). The instrument operates nominally since the beginning of the mission and its operational performances are well in line with the specifications [22]–[24]. The nominal resolution of the ScaRaB footprint at nadir is 40 km and is detailed in [18].

The stability of the instrument is monitored by the CNES on a daily basis and so far, the Megha-Tropiques instruments have shown remarkable stability [25]. The use of geophysical AQ:6 targets like deep convective clouds (DCC) has been shown to be useful for geophysical calibration and cross-calibration of either broad radiometers [26], [27]. It is used here to showcase the relative stability of the channel 4 to that of the longwave channel. Fig. 3 shows the ratio between the radiance in channel 4 and channel 1 over the studied period for various deep convective regimes. The two channels of the instrument show no sign of relative degradation and a very steady behavior. Comparisons with the Clouds and the Earth's Radiant Energy System (CERES) instrument using dedicated collocation campaigns [28] further indicate a very good agreement between the two instruments' longwave channels [29].

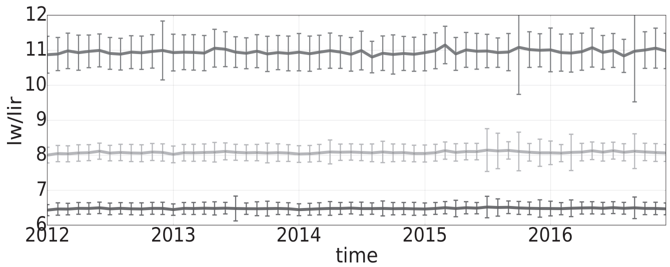

Fig. 3. Evolution of the ratio between measured radiance in the longwave band and in the IR channel of ScaRaB over the 2012–2016 period for various deep convective regimes. The blue curve corresponds to an IR radiance lower than 2.25 $W \cdot m^{-2} \cdot sr^{-1}$ corresponding to a 187 K BT, the yellow one lower than 4.25 $W \cdot m^{-2} \cdot sr^{-1}$ (207.4 K), and the red curve corresponds to an IR radiance lower than 7.75 $W \cdot m^{-2} \cdot sr^{-1}$ (224.5 K).

The ScaRab instrument is also thermally controlled and is not impacted by icing events as shown in the monitoring of the instrument performances [22], [23]. The combination of an accurate and stable instrument makes it a well-suited reference to adjust the geostationary data.

Here we use the so-called level 2B products that consist of a 0.5° regularly gridded instantaneous directional radiances ($W \cdot m^{-2} \cdot sr^{-1}$). The original measurements are averaged on the regular grid using a statistical technique and the point spread function of the instrument [30]. Since 2011, the availability of this product is about 99.9%, making it a useful resource as a reference instrument for the spectral homogenization of the GEOring data. Note that unlike sun-synchronous platforms, the precessing orbit of Megha-Tropiques samples all the local times every 51 days allowing the collocation with the geostationary data all through the day and then the correction of the midnight IR anomaly [10], [18], [31]. The low inclination at the equator (20°) and high altitude of flight (865 km) also allow high repetitive measurements in the tropics [18].

III. Homogenous Level 1c IR Data Set for the Tropics for 2012–2016

A. Homogenization of the Temporal Resolution

Given the requirements for cold cloud studies (see Section I), the lack of temporal resolution homogeneity between the geostationary imagers is accounted for by using a 30-min temporal frequency for all the platforms, preventing the use of MTSAT data in the southern hemisphere.

B. Homogenization of the Spatial Resolution

A common equal angle grid of 0.04° × 0.04° has been selected for all the platforms to account for this source of inhomogeneity. This resolution is very close to the native resolution of GOES-13, GOES-15, MTSAT-2, and Meteosat-7 data. The regridding process is performed by applying the inverse distance weighting method in the radiance space with a maximum search radius corresponding to the sum of half of the geostationary spatial resolution for a given pixel plus a half of the equal angle grid resolution. Then, the average radiance is transformed in BT using the Planck function in order to account for its nonlinearity.

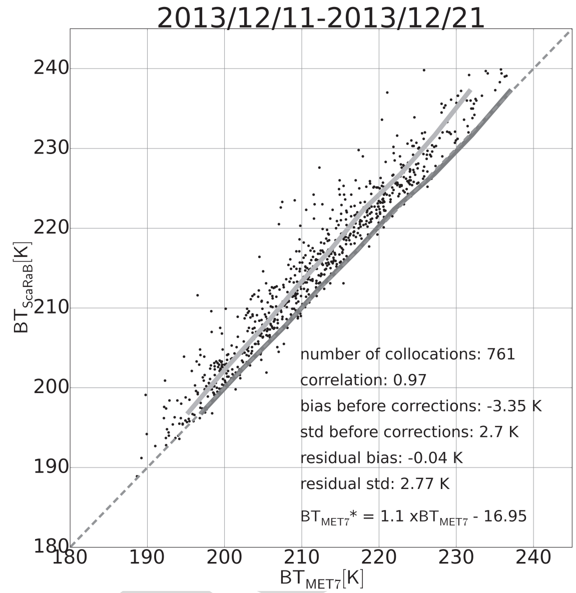

Fig. 4. Scatter plot between BT_{MET7} and BT_{ScaRaB} obtained after the filtering procedure over a ten-day period starting in 2013/12/11 for BT in the range [180–240 K]. The orange line corresponds to the average BT for each 5 K bin. The blue line corresponds to the residual bias.

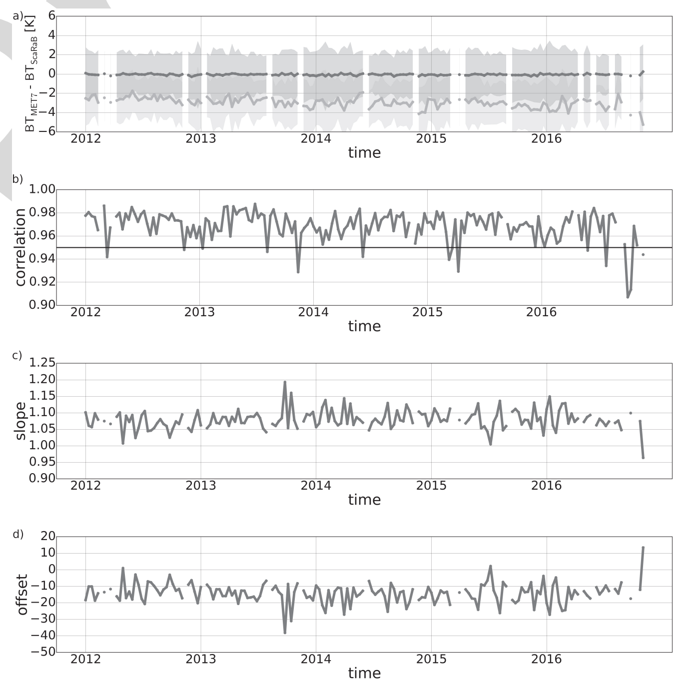

Fig. 5. (a) Time series of decadal initial BT bias (orange) and corrected BT bias (blue) for Meteosat-7 IR observations with respect to ScaRaB in the range [180–240 K]. The filled and transparent areas in orange and blue represent the standard deviations: (b) Time series of decadal linear regression correlations, (c) slope, and (d) offset between the ScaRaB and the Meteosat-7 IR observations in the range [180–240 K].

C. Intercalibration and Spectral Normalization

1) Regression Technique: The use of a common low earth-orbiting satellite, carrying an IR radiometer to anchor each of the platforms to a common reference data set, forms the basis of the different intercalibration and normalization

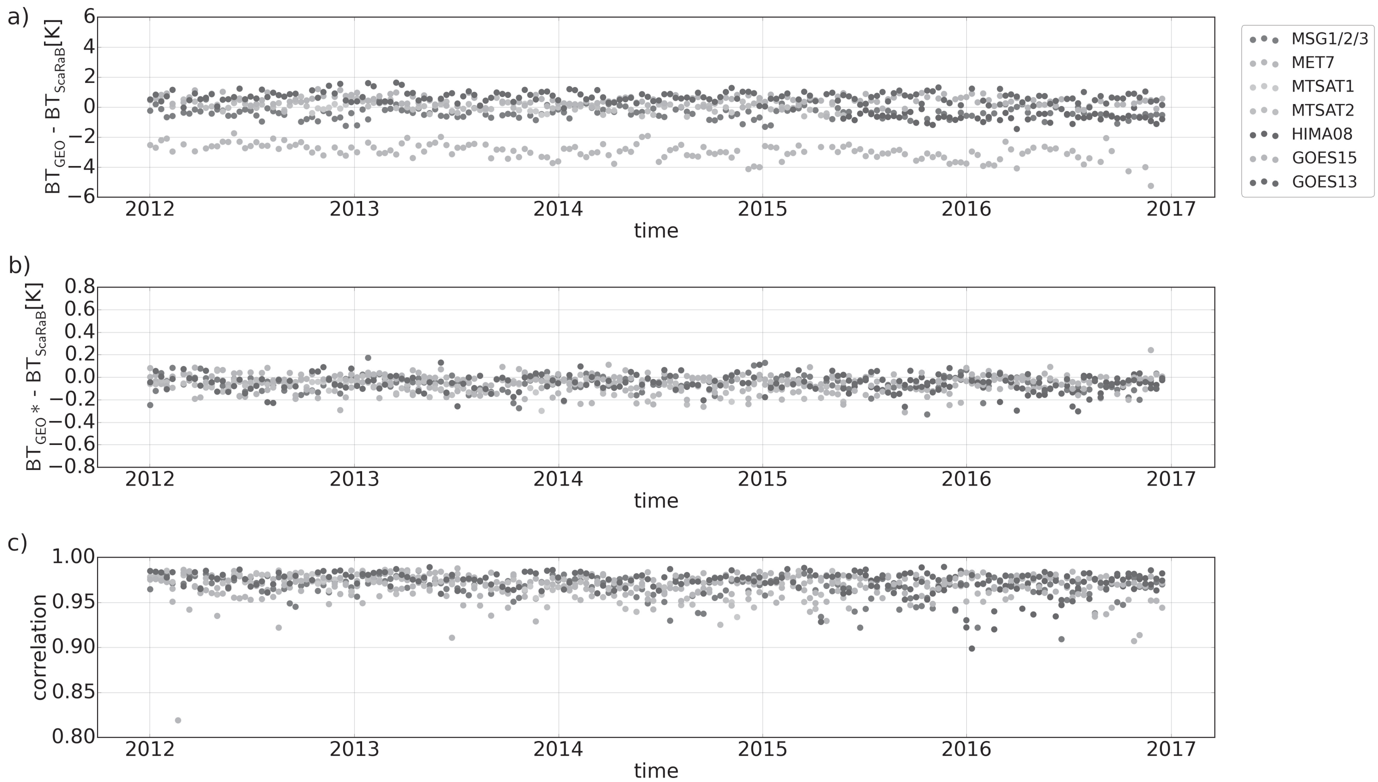

Fig. 6. (a) Time series of initial BT bias of geostationary IR observations with respect to ScaRaB in the range [180–240 K]. (b) Time series of BT bias between the geostationary IR observations and the ScaRaB observations in the range [180–240 K] after spectral and calibration corrections. (c) Time series of correlations between the ScaRaB and the geostationary IR observations in the range [180–240 K]. Each dot corresponds to a ten-day period.

efforts listed in Table I [14], [32] or under the GSICS calibration procedure [7]. Regression-based techniques are the most commonly used approaches. The difficulty arises in building the pairs (space/time/angular collocation) as well as in selecting the pairs of observations that will be regressed. This selection can have a strong impact on the result. Hence, it has been noted that the original ISCCP intercalibration was skewed toward a warm scene due to the implementation of the pairs selection filter prior to the regression computation, yielding a ∼4 K cold bias on the cold part of the spectrum [33]. Similarly, most of the tropical observations are located over large BT values and only a few of them are explained by DCCs. As the larger population of collocations is explained by high BT, the GSICS corrections are optimized for clear sky conditions and are not well suited for the cold cloud scenes [7]. A specific homogenization of the IR geostationary database is then required to fit with the objective of cold cloud tracking applications. This homogenization consists of a spectral normalization as well as an intercalibration of the various geostationary imagers focused on high cold clouds and on cold BTs. For this purpose, the BTs from the geostationary imagers are calibrated and spectrally normalized against the ScaRaB channel 4 measurements. The final data set then consists of a 10.5–12.5 μm IR equivalent BT. Calibration uncertainty is expected to be within 1 K, which is the typical error for operational satellite calibration [34]. Contrary to other geostationary imagers, the correction of the Meteosat-7/MVIRI imager is restricted to an intercalibration procedure, since its broad SRF is similar to the ScaRaB/channel 4 and both of them are centered on 11.5 μm.

2) Selection of the Data Match-Ups for the Regression: The IR geostationary data from all the platforms are first remapped from their native formats to a regular lon/lat 0.5° grid every 30 min to allow direct comparison with the ScaRaB/L2B data. Prior to computing the averaged radiance and the associated spatial standard deviation for each 0.5° grid point, the BTs of each geostationary platform are converted in radiances ($mW \cdot m^{-2} \cdot sr^{-1} \cdot cm^{-1}$) by applying the Planck function. The information on geostationary scan-time is also indicated for every grid point. The collocation between the ScaRaB-L2B observation and the IR 0.5° × 0.5° gridded geostationary data is reached when both view the same scene with a predefined time delay and similar viewing geometry. The predefined criteria are.

1) A maximum VZA of 20° and 26°, respectively, for the ScaRaB and the geostationary observation, to ensure alignment of the collocated pixels in viewing geometry and to avoid limb-darkening issues [35].
2) A maximum time delay of 10 min between two collocated pixels, which is a tradeoff between a relevant number of match-ups to populate the decadal regressions and the best possible temporal precision.
3) The IR-gridded radiances are regressed in units of temperature.

As we focus on high cold clouds scenes, we have developed a filtering procedure that keeps more collocation scenes at a colder temperature. Indeed, a bulk of collocations occurs at

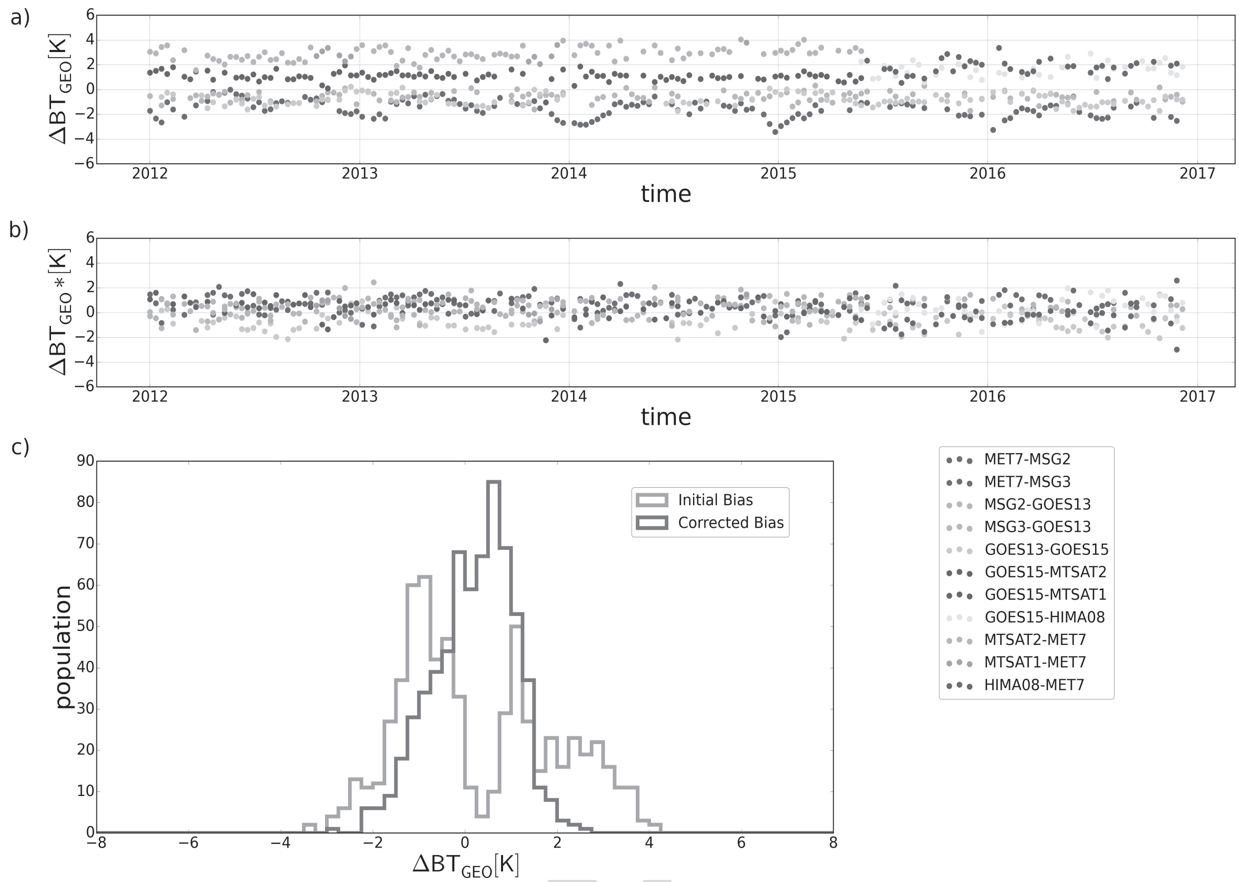

Fig. 7. (a) Time series of initial BT bias between pairs of geostationary platforms observing common areas with an equivalent VZA in the range [180–240 K]. (b) After spectral and calibration corrections; each dot corresponds to a ten-day period. (c) Distribution of the bias before and after corrections over the 2012–2016 period for all the pairs of geostationary platforms for all the ten-day periods.

a warmer temperature and displays a lower standard deviation [33]. To separate the high cold cloud population from the warmer targets in the scatterplot, thresholds are applied to the GEO standard deviation that depends on the BT. Pixels presenting a $BT_{GEO} > 240$ K are rejected if their standard deviations are larger than 0.5 K and pixels with $BT_{GEO} < 240$ K are kept if their standard deviations are lower than 2 K. Besides separating the high cold cloud population from clear sky pixels, this filtering procedure ensures that heterogeneous moving objects do not contaminate the collocation scenes and that the two instruments observe the same high cloud target. Assuming also that the IR radiometers onboard geostationary platforms have a linear response when observing high cold cloud homogeneous scenes [8], [36], the calibration and spectral normalization corrections are then based on linear regressions computed over a 180 –240 K range. For this, the collocated BT_{GEO} and BT_{ScaRaB} are binned and averaged for every BT_{ScaRaB} interval of 5 K from 180 to 240 K. The regression coefficients are then computed over these binned data every ten days and over a ten-day period. This is required to ensure statistical robustness but prevent higher frequency variation (<10 days) of the calibration issues (due to decontamination for instance) to be accounted for. As shown below, such higher frequency effects do not impact the residuals of the regression. Correlations are used to determine the ten-day period that might have match-ups errors. If the correlations are lower than 0.95 or if the population of collocations does not exceed ten matchups, we consider that the linear regression cannot be computed and that every ten-day period is removed from our analysis. In this case, the previous regression coefficients are replicated.

3) Results: Fig. 4 shows an example of such a regression computed from 761 collocated pixels between the Meteosat-7/MVIRI imager and the Megha-Tropiques/ScaRaB observations acquired over a ten-day period from 2013/2012/2011 and for a range between 180 and 240 K. The 11.5 μm channel of Meteosat-7 exhibits a large negative bias (−3.35 K) for this considered BT and for this specific period. The blue line shows the regression fit given by a slope of 1.11 and an offset of −16.95 K. The correction has produced a very low residual bias, which averages at −0.04 K over this decadal period, and the correlation higher than 0.97 between the two data sets shows the high quality of the regression computation. Fig. 5(a) shows the time series of difference between Meteosat-7/MVIRI and ScaRaB before and after calibration over the 2012–2016 period. The Meteosat-7 BT is corrected every ten days using the slopes and offset computed from the linear regression. Over the period and for the specific Meteosat-7 geostationary platform, 12% of the decadal scatterplots are excluded from our analysis following

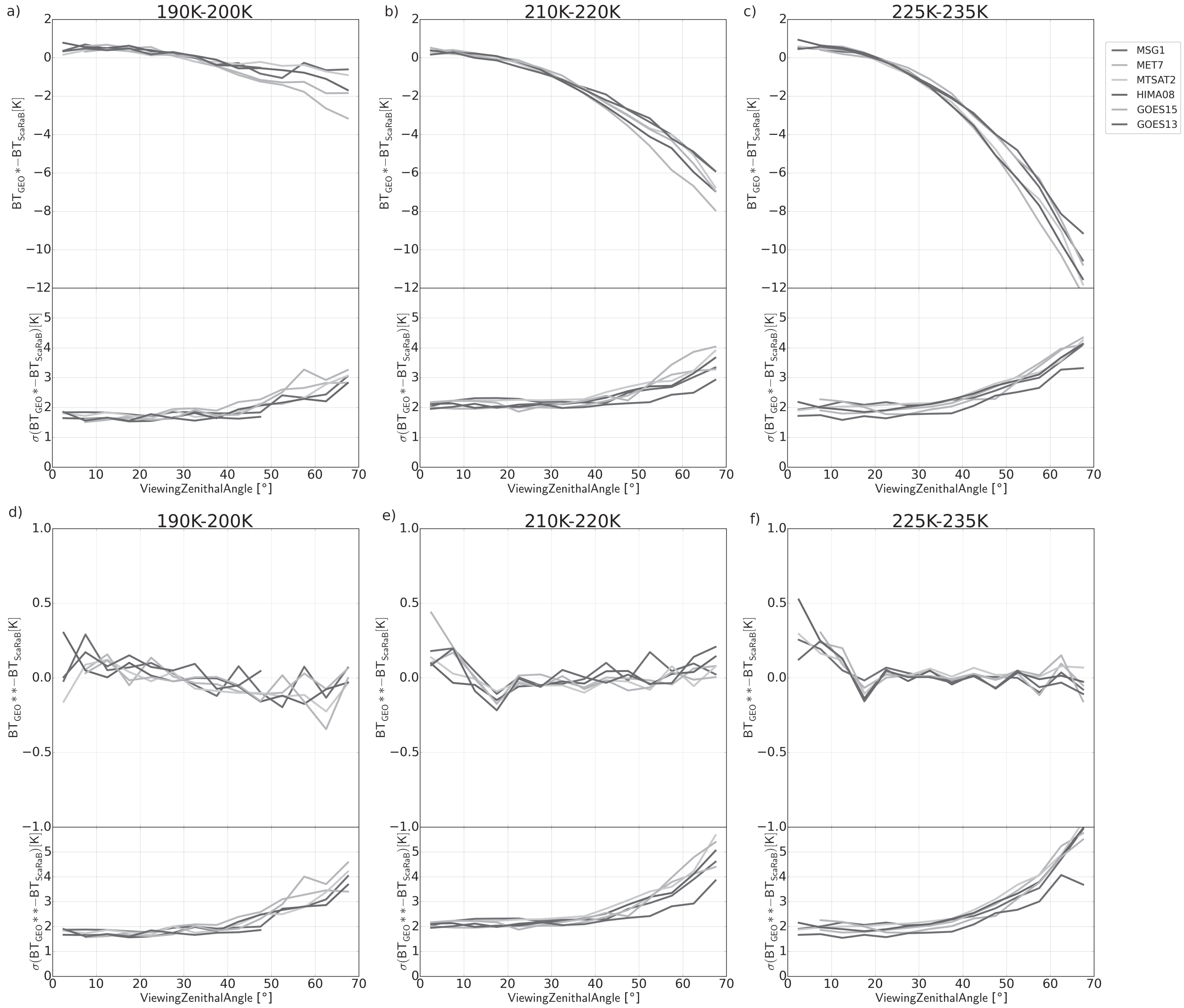

Fig. 8. Variation of the BT bias and the corresponding standard deviation between the GEO and the SCARAB observations according to the geostationary VZA, for a $VZA_{ScaRaB} < 20°$ and for three different ranges of BT_{ScaRaB}. (a)–(c) Before VZA corrections. (d)–(f) After VZA corrections.

the filtering procedure [Fig. 5(b)] and 87 405 collocations have then been used to compute the decadal regressions. One can observe that over the 2012–2016 period, and before the corrections, the Meteosat-7/MVIRI exhibits a negative bias, averaging at −2.98 K and negatively increasing slightly with time due to contamination on the optics. This radiometric issue has been fully documented in [7]. The variations of the slopes and offsets are relatively stable over the period [Fig. 5(c) and (d)], showing the robustness of the methodology. After applying the calibration correction, the residual bias is very smooth, stable, and close to zero over the whole period. The calibration and spectral normalization corrections are applied on all the geostationary platforms available over the 2012–2016 period. The results have been obtained over the entire period, and for all the geostationary platforms by filtering 8% of the decadal scatterplots which did not pass our quality control [Fig. 6(c)], leading to a comparison of around 655 000 collocations. Fig. 6(a) shows the time series of the decadal initial bias in BT for all the geostationary imagers with respect to the ScaRaB observations in the range 180–240 K. Over the 2012–2016 period, the Meteosat-7/MVIRI exhibits the highest error as discussed previously. It is also to be noted that the MSG/SEVIRI imager shows a relatively high negative bias (−1.39 K) to be compared to the other instruments whose biases are mainly in the range −0.5–0.5 K over the entire period. While the calibration issues only explain the bias between Meteosat-7 and ScaRaB, the differences of temperature between ScaRaB and the other geostationary platforms can be explained by both a poor calibration and some differences in the SRF. The results of the intercalibration and spectral normalization are shown in Fig. 6(b). Over the entire period and for all the geostationary platforms, the decadal

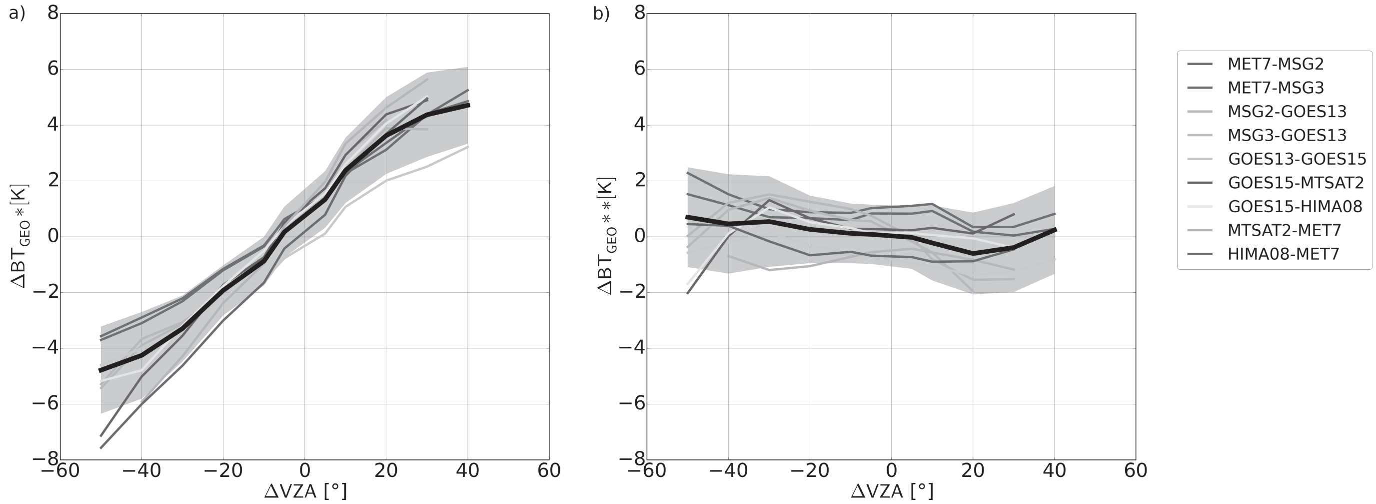

Fig. 9. Variation of the BT bias according to the VZA differences between pairs of geostationary platforms observing common areas and for BT_{ScaRaB} in the range [180–235 K]. (a) Before VZA corrections. (b) After VZA corrections. The BT bias and its standard deviation for all the pairs of geostationary platforms are represented respectively by the black line and the filled area in gray over the 2012–2016 period for all the ten days.

residual bias indicates a very low and stable bias, around 0 K, with a standard deviation lower than 0.08 K between BT_{ScaRaB} and BT_{GEOS}. The corrections are then directly applied to the original geostationary data.

To fully describe the impact of the ScaRaB calibration and spectral corrections, an independent validation has been developed. The bias of uncorrected and corrected BT_{GEO} is then computed in the range of 180–240 K every ten days between pairs of neighbored geostationary platforms observing common areas and sharing an equivalent VZA (Fig. 7). Indeed, for two adjacent geostationary satellites, the BT bias at the middle of the overlap region should average to zero, due to the similar geometry for both platforms. Fig. 7(a) shows the time series of decadal mean differences between uncorrected BTs of each pair of geostationary satellites. Each color represents a pair of geostationary platforms. Results indicate a scatter of the decadal bias between −4 and 4 K. The maximum bias occurs for the BT differences between MTSAT-1/2 and Meteosat-7, which averages at 2.9 K from the beginning of 2012 to June 2015. The bias between uncorrected BT_{MET-7} and $BT_{MSG-1/2/3}$ exhibits a relatively high bias (−1.62 K on average) and is distinguishable from the other pairs of geostationary satellites, in contrast to its relatively high seasonal variations. The distribution of the decadal initial bias for all the geostationary platforms over the 2012–2016 period [Fig. 7(c)] reveals a multimodal distribution, which averages at 0.25 K and displays a standard deviation of 1.65 K. Fig. 7(b) shows that the corrections applied to the geostationary IR observations improve the error as well as the disparity of the scatter plot over the whole period and for all the geostationary platforms. These results are confirmed by the Gaussian distribution of the decadal bias for corrected BT_{GEOS} shown in Fig. 7(c), which averages at 0.19 K with a standard deviation of 0.87 K. The resulting geostationary satellite calibration residuals specifications are hence well within the 1 K limit previously mentioned and demonstrate the importance to develop a correction procedure for the geostationary IR observations at cold temperatures.

D. Limb-Darkening Adjustment

1) Methodological Considerations: To complete the homogenization procedure of the geostationary database, we focus now on the dependence of the BT_{GEOS} on the VZA. This issue, also called limb darkening, corresponds to a decrease in the temperature as the VZA increases. The greater optical path length of the absorbing atmosphere, as the VZA increases, results in a larger atmospheric absorption. Indeed, a longer optical path length contains much more water vapor and ozone explaining the observation of colder temperatures [35], [37], [38]. Cloudy scenes imply a second mechanism in the VZA issues [35]. A geometric effect may also be involved when the sides of the clouds obstruct the Earth's emitted radiation at a large VZA. Some studies on these geometric effects discussed the different configurations of cloud fields [39]. To prevent an erroneous analysis between meteorological situations, which occurred at nadir and at a large VZA, the BTs have to be limb-adjusted. Some studies have been carried out to limb adjust the IR observations for cloudy regions by establishing empirical limb correction functions, depending on the cosine of zenith angle from the radiative transfer model for low earth orbit platforms [39] and IR geostationary observations [40]. However, it has been shown [41] that the corrections developed by [39] underestimate the observed BTs. The variation of the radiance, according to the zenith angle, is approximated in the CLAUS data set, by applying a function of the cosine of the zenith angle. Another way to face the limb-darkening issues is to use observations from low earth orbit platforms. Limb-correction algorithms have been developed for microwave observations from the AMSU-A and are based on a physical-statistical methodology [37]. The limb-darkening problem has also been

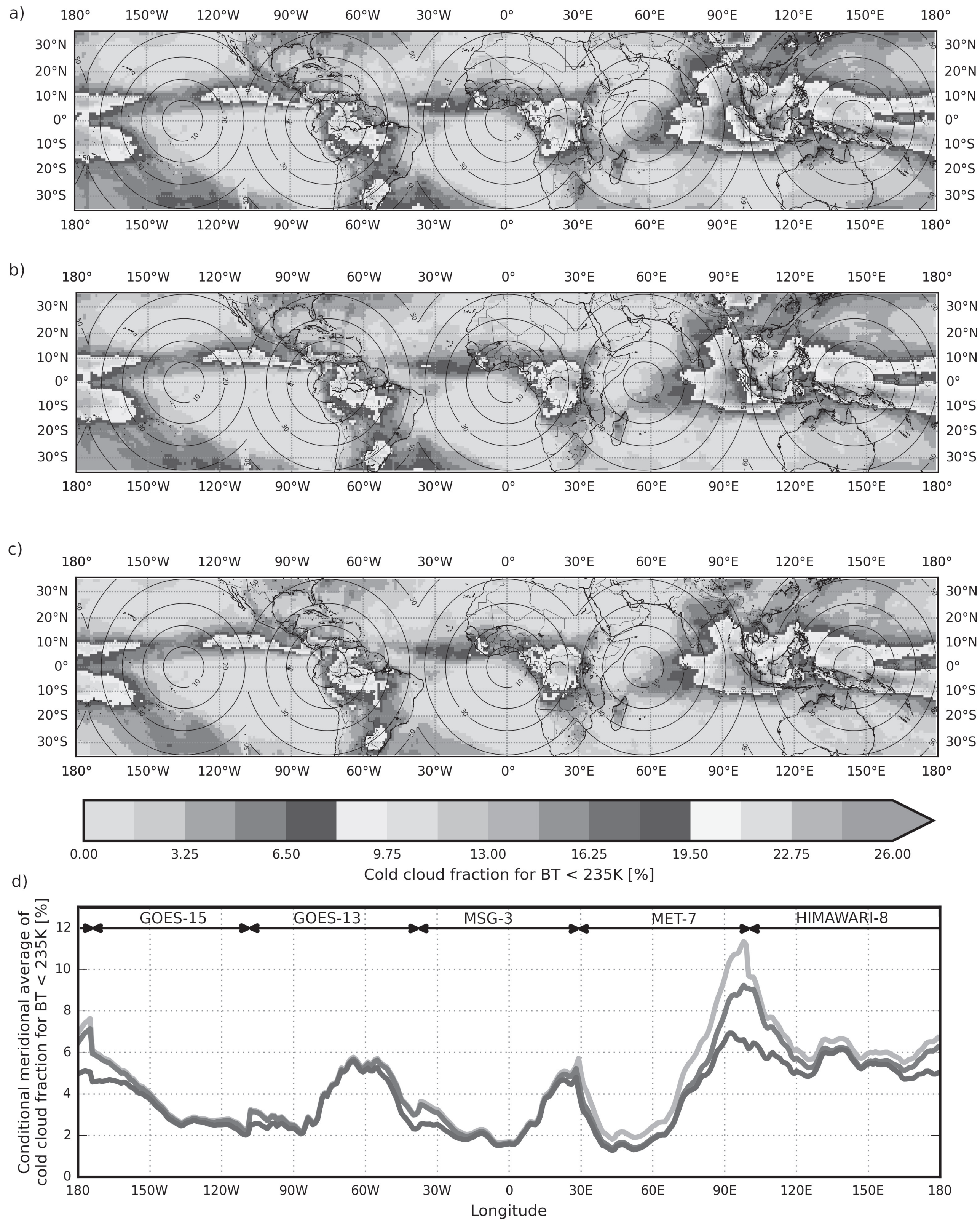

Fig. 10. Map of the mean cold cloud fraction (%) for $BT_{GEO} < 235$ K over 2016 (a) by using the initial BT_{GEO} before any corrections, (b) by using the calibrated and spectrally corrected BT_{GEO}, and (c) after applying the VZA corrections on BT_{GEO}. The black circles represent the different levels of VZA. (d) Conditional meridional average of the cold cloud fraction for $BT_{GEO} < 235$ K before any corrections (orange line), after applying the calibration and spectral corrections (blue line) and after applying the VZA corrections (red line).

explored by comparing the radiances from the geostationary platforms with observations from polar orbiter platforms [40]. Some limb-darkening corrections have been computed from collocated pairs of GOES platforms (GOES-8/GOES-10) and Meteosat platforms (Meteosat-5/Meteosat-7) [35]. They proposed a two-step correction. First, a correction table of the BT_{GEO} as a function of VZA is applied to BT_{GEO} only for observations in the tropics. For mid-latitude regions, an additional correction is applied to tackle the latitudinal and seasonal dependence of BT_{GEO}. This dependence is explained by a smaller contrast between the cloud top and the Earth's surface in mid-latitudes than over the tropics. This limb-darkening correction is used in GridSat and ISCCP data sets [4]. However, this methodology is likely to suffer from limitations to be used to homogeneously limb adjust a fleet of geostationary satellites. Indeed, the limb adjustment, developed in the 2000s and empirically derived from a combination of a specific and limited set of instruments, may also be biased for other and new generation of geostationary instruments [12]. Moreover, the computation of the limb-darkening correction is limited by the range of VZA, due to the combination of the fixed location of geostationary satellites inducing few observations of cold BT_{GEO}.

It appears important, for this article, to tackle limb-darkening issues on geostationary satellite per geostationary satellite over the full time period by using a common reference, such as the IR observation from the ScaRaB instrument. This correction focuses on cold clouds monitored by the IR imagery of geostationary satellites previously intercalibrated and normalized into a 10.5–12.5 μm IR equivalent BT, called BT^{*}_{GEO}. For this purpose, we perform for each GEO platform a collocation procedure between the regular lon/lat 0.5° and corrected IR geostationary data, presented previously, and the ScaRaB/L2B IR observation over the entire 2012–2016 period. The collocation procedure is applied under some criteria. Where the zenithal angles of ScaRaB do not exceed 20°, the geostationary zenith angles can range from 0° to 70°. The collocation is also performed with a time delay of less than 10 min between the GEO and the ScaRaB observations and for BT_{ScaRaB}, which does not exceed 235 K for standard deviations lower than 2 K.

GEO-ScaRaB match-ups are binned into geostationary zenith angle intervals of 2° and for zenith angles ranging from 20° to 70°. For GEO VZAs lower than 20°, a unique limb correction is performed. Moreover, to ensure a relevant sample size on each 2° zenith angle bin, the regressions are applied annually. For each zenith angle interval, the collocated $BT_{GEO}*$ and BT_{ScaRaB} are binned and averaged for every BT_{ScaRaB} interval of 5 K, from 180 to 235 K. To filter corrupted collocated points, the binning procedure is performed when at least ten samples are present. The limb correction then consists of applying annual regressions between the binned GEO and ScaRaB data for every 2° zenith angle bin and for each geostationary platform. A second-order polynomial regression has been preferred over the linear regression, due to slight improvements in the minimization of the residuals.

2) Results: Fig. 8(a)–(c) shows the variation of the initial bias between each GEO platform and ScaRaB, according to the VZA for different bins of ScaRaB temperatures and over the 2012–2016 period. First, one can observe a negative increase in the bias as the VZA increases, whatever the range of BT. For VZA lower than 30°, the absolute bias seems to be lower than 1 K, whatever the BT_{ScaRaB} is. However, we can observe drastic differences in the bias evolution depending on the BT_{ScaRaB} bin. Indeed, at warmer BT_{ScaRaB} [225–235 K], the negative increase in the bias according to the VZA is more pronounced than for colder values of BT_{ScaRaB} [190–200 K]. For a VZA at 40°, the bias averages at -0.63 K for BT_{ScaRaB}, ranging from 190 to 200 K and for all the GEO platforms, while the bias averages at -2.9 K for BT_{ScaRaB} greater than 225 K and for a similar VZA. It is also to be noticed that the disparity of the bias among GEO platforms increases with the VZA. Thus, at a 60° zenith angle and for the 225–235 K range, the bias varies from -7.4 to -9.5 K for GOES-15 and Meteosat-7, respectively. Such large errors have been previously reported for an older Meteosat first-generation satellite (Meteosat-4) compared to NOAA/AVHRR reference [27]. Note that the uncertainty does not increase much with the BT but increases with the VZA. Fig. 8(d)–(f) shows the results of the limb-darkening corrections according to the variation of the zenith angle for all the geostationary platforms and for different ranges of BT_{ScaRaB}. Over the whole range of ScaRaB BTs, the residual biases average at 0 K, regardless of the geostationary platform and the zenith angles. These results demonstrate the capability of the limb-darkening correction methodology we have developed. An independent validation is provided in Fig. 9 by comparing pairs of geostationary platform observations. It shows the variation of the decadal biases of $BT_{GEO}*$ between pairs of geostationary satellites, according to the difference of their VZAs (ΔVZA), before and after applying limb-darkening corrections. A ΔVZA of 0° means that two adjacent geostationary platforms observe the same region with an equivalent VZA. On the contrary, a large ΔVZA indicates that a given geostationary platform observes a region with a nadir zenith angle, while the adjacent geostationary platform monitors the same region with a limb zenith angle. Before applying the zenith angle corrections, we can observe an increase of $BT_{GEO}*$ bias for all the platforms from ~ -5 to ~ 5 K as the ΔVZA moves from $-50°$ to 40° [Fig. 9(a)]. The standard deviation, on its side, varies between 0.86 K for a low ΔVZA and 1.57 K for large ΔVZA. Results indeed indicate a larger disparity of the $BT_{GEO}*$ biases between pairs of geostationary satellites for large ΔVZA. After applying the zenith angle correction [Fig. 9(b)], the $BT_{GEO}**$ bias is relatively stable and averages at 0.09 K with a standard variation of 1.43 K, regardless of the variation of ΔVZA. The standard deviation varies from 1.05 to 1.78 K for low and large ΔVZA, respectively. Note that when the limb-darkening issue is clearly improved and corrected, the standard deviation for a low VZA is a little larger than before applying the VZA correction.

IV. Discussion and Conclusion

In summary, a level 1c IR GEOring data set is introduced. This data set is a consistent 10.5–12.5 μm IR equivalent BT data set, with a homogeneous recalibration, a 0.04° × 0.04° spatial resolution, a 30 min common time resolution, and a correction for limb effect. The data set covers the 2012–2016 period. The global homogeneity of the IR GEOring data set, regardless of the variation of VZA, is then characterized by a standard deviation of 1.43 K within any of two geostationary satellites.

As discussed in the Introduction section, global geostationary IR observations provide useful resources to carry out studies on convective systems. Cold cloud tracking algorithms usually delineate cold clusters by applying a 235 K threshold on IR geostationary data. To evaluate the impact of the geostationary IR data homogenization on high cold clouds, we compute the cold cloud fraction. The fraction is determined by applying a 235 K threshold on the initial BT_{GEO} before any corrections, on the spectrally adjusted and calibrated BT_{GEO} and finally on the VZA corrected IR data for the 2016 period and over the entire tropics. The computations are performed by using the selected configuration of the geostationary fleet and the map of cold cloud fraction provided on a $1^\circ \times 1^\circ$ grid [Fig. 10(a)–(c)]. Before corrections, a local maximum of cold cloud fraction reaching 26% is seen in the Meteosat-7 area over the west coast of the Indo–China peninsula. However, the calibration correction allows to attenuate this fraction which falls to 22%. Also, note that this region is observed by Meteosat-7 with a VZA of 47°. After the limb-adjustment procedure, the value of cold cloud fraction for this specific region decreases to 17%. The maximum of cold cloud fraction is now located over the warm pool and is observed by the HIMAWARI-8 platform. One can also see that the local maximum of cold cloud fraction over the Tibetan plateau is strongly attenuated with all the corrections. Before applying the homogenization procedure, one can observe some steps of the conditional meridional average of cold cloud cover at the boundary of Meteosat-7 and HIMAWARI-8 and between HIMAWARI-8 and GOES-15, reaching 1.65% and 1.47%, respectively [Fig. 10(d)]. The combined corrections improve these issues and show a cold cloud cover exhibiting a smoother transition from one platform to another. Fig. 10(d) shows similar cold cloud covers for low VZA between a unique calibration/spectral correction and the combined calibration/spectral and VZA corrections, while one can observe a decrease in cold cloud cover for large VZA between the two corrections.

The extension of the current database beyond 2016 is under consideration. The configuration of the fleet, nevertheless, drastically changes in 2017 with the end of operation of Meteosat-7 and the arrival of MSG-1 in February on a shifted position, although not fully covering the Indian Ocean. Tests are needed to explore the sensitivity of the database to this new configuration. The use of INSAT-3D is also contemplated as a better way to bridge MSG-1 and HIMAWARI-8 data. GOES-R has become operational and the stream of GOES-16 replaces GOES-13 in December 2017. Similarly, GOES-17 is now operational as the new GOES west coverage replacing the GOES-15 platform from February 2019.

Up to the end of 2018, the Megha-Tropiques mission has been operated nominally granting the possibility of extending the present effort up to that time. While the present work relies on the ScaRaB instrument onboard Megha-Tropiques, it can easily be applied to alternative IR reference observations, from hyperspectral sounders, for instance. This article indicates that the final calibrated and limb-adjusted IR observations for $BT < 240$ K can be homogeneous throughout the GEOring with less than 1.5 K standard deviation, and that further future efforts should strive for such, or better, accuracy.

Acknowledgment

The authors would like to thank the ESPRI/IPSL team for providing computing and storage resources. They also thank the DWD as well as the French data center AERIS for their help in accessing the data (GEOring, ScaRaB). They also thank G. Urbani and C. Bovalo for their help in handling the geostationary satellite data archive. They further acknowledge M. Dejus, Project Manager at CNES, and his team for their help on the technical aspects of ScaRaB. The ScaRab L2B is available in the ICARE data and service center with an *Anonymous* File Transfer Protocol (ftp://ftp.icare.univ-lille1.fr/SPACEBORNE/SCARAB/MT1_L2B-FLUX-SCASL1A2_0.5deg.v2.01/). The calibration coefficients and the limb-adjustment coefficients are available at the following DOI: https://doi.org/10.14768/20191125.

References

[1] R. A. Schiffer and W. B. Rossow, "The International Satellite Cloud Climatology Project (ISCCP): The first project of the World Climate Research Programme," *Bull. Amer. Meteorol. Soc.*, vol. 64, no. 7, pp. 779–784, Jul. 1983.

[2] M. L. Salby, H. H. Hendon, K. Woodberry, and K. Tanaka, "Analysis of global cloud imagery from multiple satellites," *Bull. Amer. Meteorol. Soc.*, vol. 72, no. 4, pp. 467–480, Apr. 1991.

[3] G. J. Huffman *et al.*, "The Global Precipitation Climatology Project (GPCP) combined precipitation dataset," *Bull. Amer. Meteorol. Soc.*, vol. 78, no. 1, pp. 5–20, 1997.

[4] K. R. Knapp *et al.*, "Globally Gridded Satellite observations for climate studies," *Bull. Amer. Meteorol. Soc.*, vol. 92, no. 7, pp. 893–907, Jul. 2011.

[5] R. A. Kohrs, M. A. Lazzara, J. O. Robaidek, D. A. Santek, and S. L. Knuth, "Global satellite composites—20 years of evolution," *Atmos. Res.*, vols. 135–136, pp. 8–34, Jan. 2014.

[6] P. Zhang, K. Holmlund, M. Goldberg, and J. Lafeuille, "The Global Space-based Inter-Calibration System (GSICS)," in *Proc. IEEE Int. Geosci. Remote Sens. Symp. (IGARSS)*, Jul. 2016, pp. 5522–5523.

[7] T. J. Hewison *et al.*, "GSICS inter-calibration of infrared channels of geostationary imagers using Metop/IASI," *IEEE Trans. Geosci. Remote Sens.*, vol. 51, no. 3, pp. 1160–1170, Mar. 2013.

[8] D. R. Doelling *et al.*, "Geostationary enhanced temporal interpolation for CERES flux products," *J. Atmos. Ocean. Technol.*, vol. 30, no. 6, pp. 1072–1090, Jun. 2013.

[9] T. J. Hewison and J. Muller, "Ice contamination of Meteosat/SEVIRI implied by intercalibration against Metop/IASI," *IEEE Trans. Geosci. Remote Sens.*, vol. 51, no. 3, pp. 1182–1186, Mar. 2013.

[10] B. Scarino, D. R. Doelling, C. Haney, K. Bedka, and P. Minnis, "Utilizing the precessing orbit of TRMM to produce hourly corrections of geostationary infrared imager data with the VIRS sensor," *Proc. SPIE*, vol. 10403, Aug. 2019, Art. no. 104030H.

[11] G. J. Robinson and K. I. Hodges, "Cloud archive user service user guide," Tech. Rep., 2005, p. 16. AQ:8

[12] K. R. Knapp, "Gridded satellite B1 FCDR—Monthly means," Tech. Rep., 2016.

[13] J. E. Janowiak, R. J. Joyce, and Y. Yarosh, "A real-time global half-hourly pixel-resolution infrared dataset and its applications," *Bull. Amer. Meteorol. Soc.*, vol. 82, no. 2, pp. 205–217, Feb. 2001.

[14] Y. Desormeaux, W. B. Rossow, C. L. Brest, and G. G. Campbell, "Normalization and calibration of geostationary satellite radiances for the International Satellite Cloud Climatology Project," *J. Atmos. Ocean. Technol.*, vol. 10, no. 3, pp. 304–325, Jun. 1993.

[15] T. Fiolleau and R. Roca, "An algorithm for the detection and tracking of tropical mesoscale convective systems using infrared images from geostationary satellite," *IEEE Trans. Geosci. Remote Sens.*, vol. 51, no. 7, pp. 4302–4315, Jul. 2013.

[16] M. Schröder, M. König, and J. Schmetz, "Deep convection observed by the Spinning Enhanced Visible and Infrared Imager on board Meteosat 8: Spatial distribution and temporal evolution over Africa in summer and winter 2006," *J. Geophys. Res.*, vol. 114, no. D5, pp. 1–14, 2009.

[17] B. E. Mapes and R. A. Houze, "Cloud clusters and superclusters over the oceanic warm pool," *Monthly Weather Rev.*, vol. 121, no. 5, pp. 1398–1416, May 1993.

[18] R. Roca *et al.*, "The Megha-Tropiques mission: A review after three years in orbit," *Frontiers Earth Sci.*, vol. 3, p. 17, May 2015.

[19] R. Kandel *et al.*, "The ScaRaB earth radiation budget dataset," Natural Resour. Canada/ESS/Sci. Tech. Publishing Services, Tech. Rep., 1998. [AQ:9]

[20] J.-P. Duvel *et al.*, "The ScaRaB-Resurs Earth radiation budget dataset and first results," *Bull. Amer. Meteorol. Soc.*, vol. 82, no. 7, pp. 1397–1408, Jul. 2001.

[21] M. Viollier and P. Raberanto, "Radiometric and spectral characteristics of the ScaRaB-3 instrument on Megha-Tropiques: Comparisons with ERBE, CERES, and GERB," *J. Atmos. Ocean. Technol.*, vol. 27, no. 3, pp. 428–442, Mar. 2010.

[22] A. Rosak, T. Tremas, N. Karouche, L. Gillot, and O. Simonella, "Radiometric and geometric Scarab-Megha-Tropiques ground calibration comparison with first in orbit calibration," in *Proc. IEEE Int. Geosci. Remote Sens. Symp.*, Jul. 2012, pp. 4746–4749.

[23] N. Karouche, C. Goldstein, A. Rosak, C. Malassingne, and G. Raju, "MEGHA-TROPIQUES satellite mission: In flight performances results," in *Proc. IEEE Int. Geosci. Remote Sens. Symp.*, Jul. 2012, pp. 4684–4687.

[24] T. L. Trémas, N. Karouche, A. Rosak, A. Meygret, O. Aznay, and E. Hillairet, "ScaRaB: First results of the scanner for radiative budget on board the Indo-French satellite Megha-Tropiques," *Proc. SPIE*, vol. 8510, Oct. 2012, Art. no. 851002.

[25] R. Roca *et al.*, "Le bilan scientifique de la mission Megha-Tropiques après 8 ans dans l'espace," *La Météorologie*, no. 107, p. 36, 2019. [AQ:10]

[26] J. P. Duvel and P. Raberanto, "A geophysical cross-calibration approach for broadband channels: Application to the ScaRaB experiment," *J. Atmos. Ocean. Technol.*, vol. 17, no. 12, pp. 1609–1617, Dec. 2000.

[27] D. R. Doelling, D. Morstad, B. R. Scarino, R. Bhatt, and A. Gopalan, "The characterization of deep convective clouds as an invariant calibration target and as a visible calibration technique," *IEEE Trans. Geosci. Remote Sens.*, vol. 51, no. 3, pp. 1147–1159, Mar. 2013.

[28] G. L. Smith, Z. P. Szewczyk, K. J. Priestley, and R. Roca, "Method of comparing CERES and ScaRaB 3 measurements," in *Proc. Sensors, Syst., Next-Gener. Satellites XVI SPIE*, 2012, pp. 7193–7196.

[29] T. L. Trémas, O. Aznay, and O. Chomette, "ScaRaB and CERES-Terra: Results of the inter-comparison campaigns," *Proc. SPIE*, vol. 9973, Sep. 2016, Art. no. 99730B.

[30] N. Gif, O. Chomette, and P. Raberanto, "Co-location algorithms geophysical data projection using pixel point spread function," Megha-Tropiques Tech. Memo. 2, 2011. [AQ:11]

[31] M. Capderou, "Sampling. Comparison with other Meteorological Satellites," Megha-Tropiques Tech. Memo. 1, 2009.

[32] C. L. Brest, W. B. Rossow, and M. D. Roiter, "Update of radiance calibrations for ISCCP," *J. Atmos. Ocean. Technol.*, vol. 14, no. 5, pp. 1091–1109, Oct. 1997.

[33] K. R. Knapp, "Calibration assessment of ISCCP geostationary infrared observations using HIRS," *J. Atmos. Ocean. Technol.*, vol. 25, no. 2, pp. 183–195, Feb. 2008.

[34] M. König, J. Schmetz, and S. Tjemkes, "Satellite intercalibration of IR window radiance observations," *Adv. Space Res.*, vol. 23, no. 8, pp. 1341–1348, Jan. 1999.

[35] R. Joyce, J. Janowiak, and G. Huffman, "Latitudinally and seasonally dependent zenith-angle corrections for geostationary satellite IR brightness temperatures," *J. Appl. Meteorol.*, vol. 40, no. 4, pp. 689–703, Apr. 2001.

[36] T. H. von der Haar and S. Q. Kidder, *Satellite Meteorology—An Introduction*. New York, NY, USA: Academic, 1995.

[37] M. D. Goldberg, D. S. Crosby, and L. Zhou, "The limb adjustment of AMSU—A observations: Methodology and validation," *J. Appl. Meteorol.*, vol. 40, no. 1, pp. 70–83, Jan. 2001.

[38] Q. Liu and F. Weng, "Uses of *NOAA-16* and *-18* satellite measurements for verifying the limb-correction algorithm," *J. Appl. Meteorol. Climatol.*, vol. 46, no. 4, pp. 544–548, Apr. 2007.

[39] P. Minnis, "Viewing zenith angle dependence of cloudiness determined from coincident GOES east and GOES west data," *J. Geophys. Res.*, vol. 94, no. D2, pp. 2303–2320, 1989.

[40] N. J. Elmer, E. Berndt, and G. J. Jedlovec, "Limb correction of MODIS and VIIRS infrared channels for the improved interpretation of RGB composites," *J. Atmos. Ocean. Technol.*, vol. 33, no. 5, pp. 1073–1087, May 2016.

[41] K. I. Hodges, D. W. Chappell, G. J. Robinson, and G. Yang, "An improved algorithm for generating global window brightness temperatures from multiple satellite infrared imagery," *J. Atmos. Ocean. Technol.*, vol. 17, no. 10, pp. 1296–1312, Oct. 2000.

Thomas Fiolleau received the Ph.D. degree from Ecole Polytechnique, Paris, France, in 2010 with a thesis on the use of satellite observation to study mesoscale convective systems in the framework of the Megha-Tropiques Indo–French Satellite Mission.

He was an Associate Engineer with the Laboratoire de Météorologie Dynamique (LMD), Paris, for two years. He worked as a United Nations Educational, Scientific and Cultural Organization (UNESCO) Consultant with the Centro Nacional de Monitoramento e Alertas de Desastres Naturais (CEMADEN), Brazil, a Brazilian operational center, where he worked on the development of operational algorithms to forecast convective systems. After two years at CNRM (joint laboratory between CNRS and Météo-France), he joined the CNRS in 2016 as a Research Engineer with the Laboratoire d'Etudes en Géographie et Océanographie Spatiales, Toulouse, France. His areas of specialization are remote sensing, image processing, tropical climate and meteorology, and his researches interests are focused on the development of cloud tracking algorithms from geostationary satellites and the study of the life cycle of tropical mesoscale convective systems by using satellite observations.

Rémy Roca received the M.S. degree in fundamental physics, with major in remote sensing, and the Ph.D. degree in 2000 from Université Paris, Paris, France, with a thesis on the use of satellite observations to evaluate climate models. [AQ:12]

He was with the Scripps Institution of Oceanography, University of California, San Diego, CA, USA, for almost two years where he got familiar with image processing and cloud detection and tracking algorithms from geostationary satellites. From 2001 to 2012, he was with the Laboratoire de Météorologie Dynamique, Institut Pierre et Simon Laplace, Paris, where he was a CNRS Researcher. He was appointed a Mission Scientist of the Megha-Tropiques Indo–French Satellite Mission and took over the PIship of the mission in 2007. He is a Senior CNRS Researcher with the Laboratoire d'Etudes en Géographie et Océanographie Spatiales, Toulouse, France. His broad interests are focused on the study of the water cycle in the tropics and the use of satellite observations to investigate the tropical variability. He has more than 15 years of experience in the field of tropical climate, meteorology, and remote sensing.

Dr. Roca was the Chairman of the International Precipitation Group in 2014 and 2015, and since 2016, he has been co-leading the GEWEX/WCRP Data Analysis Panel.

Sophie Cloché received the M.S. degree in fundamental physics, with a specialization in remote sensing, and the Ph.D. degree in 1996 with a thesis on the use of satellite observations (POLDER) for cloud and water vapor detection from Université Paris, Paris, France. [AQ:13]

From 1996 to 1998, she was a Post-Doctoral Position with the Laboratoire de Météorologie Dynamique (LMD/CNRS), Paris, working on narrow to broadband conversion to estimate the radiative fluxes. From 1998 to 2001, she was as a Research Engineer, on database management for the INDOEX program, LMD. In 2001, she obtained a fix position with the CNRS, Institut Pierre-Simon Laplace (IPSL), Paris, as Research Engineer, and also involved in database management for different national and international projects (AMMA, Hymex, GEWEX-Cloud Assessment for example). She is the Co-ordinator of the scientific ground segment for the Megha-Tropiques mission and involved in the CM SAF from Eumetsat for the development of a global precipitation product. She also coordinates space activities at IPSL and she is responsible of the database management of observations at IPSL.

Dominique Bouniol received the Ph.D. degree from the University of Paris, Paris, France, in 2000, with a thesis on process-oriented use of observational data sets for understanding mesoscale storm deepening.

After 18 months in the Radar Meteorology Group, University of Reading, Reading, England, she joined the CNRS as a Researcher in 2002, first in CETP where she was involved in the implementation and exploitation of ground-based cloud radar in the framework of the Cloudnet project. She led the deployment of the airborne version of the cloud radar within the AMMA experiment in Niger and Senegal, in 2006. While she was with CNRS, she joined the CNRM (joint laboratory between CNRS and Météo-France), in 2006, where her research focuses on physical processes involved in the tropical mesoscale convective system life cycle and more generally on tropical cloud processes using both observations and modeling tools.

AQ:14

Patrick Raberanto received the Ph.D. degree in astronomy and space technology from Paul Sabatier University, Toulouse, France, in 1984.

In 1990, he joined the Laboratoire de Météorologie Dynamique (LMD), Ecole Polytechnique, Paris, as a CNRS Research Engineer and was implied in the ScaRaB project. In the framework of the Megha-Tropiques mission, he was in charge of the ScaRaB calibration, validation, and the development of the ScaRaB level-2 products. His research interests include radiometric calibration and radiative budget observation.